Fault kinematics and tectonic stress in the seismically active Manyara–Dodoma Rift segment in Central Tanzania – Implications for the East African Rift

Athanas S. Macheyeki [a,b,c], Damien Delvaux [d,*], Marc De Batist [a], Abdulkarim Mruma [c,e]

[a] *Renard Centre of Marine Geology, Universiteit Gent, Vkgr. Geologie, B-9000 Gent, Belgium*
[b] *Madini (Mineral Resources) Institute, Dodoma, Tanzania*
[c] *The University of Dar Es Salaam, Department of Geology, Dar es Salaam, Tanzania*
[d] *Royal Museum for Central Africa, B-3080 Tervuren, Belgium*
[e] *Geological Survey of Tanzania, P.O. Box 903, Dodoma, Tanzania*

Abstract

The Eastern Branch of the East African Rift System is well known in Ethiopia (Main Ethiopian Rift) and Kenya (Kenya or Gregory Rift) and is usually considered to fade away southwards in the North Tanzanian Divergence, where it splits into the Eyasi, Manyara and Pangani segments. Further towards the south, rift structures are more weakly expressed and this area has not attracted much attention since the mapping and exploratory works of the 1950s. In November 4, 2002, an earthquake of magnitude Mb = 5.5 struck Dodoma, the capital city of Tanzania. Analysis of modern digital relief, seismological and geological data reveals that ongoing tectonic deformation is presently affecting a broad N–S trending belt, extending southward from the North Tanzanian Divergence to the region of Dodoma, forming the proposed "Manyara–Dodoma Rift segment". North of Arusha–Ngorongoro line, the rift is confined to a narrow belt (Natron graben in Tanzania) and south of it, it broadens into a wide deformation zone which includes both the Eyasi and Manyara grabens.

The two-stage rifting model proposed for Kenya and North Tanzania also applies to the Manyara–Dodoma Rift segment. In a first stage, large, well-expressed topographic and volcanogenic structures were initiated in the Natron, Eyasi and Manyara grabens during the Late Miocene to Pliocene. From the Middle Pleistocene onwards, deformations related to the second rifting stage propagated southwards to the Dodoma region. These young structures have still limited morphological expressions compared to the structures formed during the first stage. However, they appear to be tectonically active as shown by the high concentration of moderate earthquakes into earthquake swarms, the distribution of He-bearing thermal springs, the morphological freshness of the fault scarps, and the presence of open surface fractures. Fault kinematic and paleostress analysis of geological fault data in basement rocks along the active fault lines show that recent faults often reactivate older fault systems that were formed under E–W to NW–SE horizontal compression, compatible with late Pan-African tectonics. The present-day stress inverted from earthquake focal mechanisms shows that the Manyara–Dodoma Rift segment is presently subjected to an extensional stress field with a N080°E direction of horizontal principal extension. Under this stress field, the rift develops by: (1) reactivation of the pre-existing tectonic planes of weakness, and (2) progressive development of a new fault system in a more N–S trend by the linkage of existing rift faults. This process started about 1.2 Ma ago and is still ongoing.
© 2008 Elsevier Ltd. All rights reserved.

Keywords: Tanzania; East African Rift; Manyara–Dodoma Rift segment; Fault kinematics; Tectonic stress; Seismotectonics

1. Introduction

Earthquake swarms of moderate magnitudes have been reported to have hit the northern Dodoma area in Central

---

Tanzania (Fig. 1) for many years. On November 4, 2002, an earthquake of Mb = 5.5 struck the same area during a session of the Tanzanian Parliament in Dodoma, causing cracks to the Parliament building. It was felt in the regions of Dodoma, Morogoro, Singida, Iringa, Mbeya and Arusha. Near Dodoma and in the Chenene Mountains in particular, several village buildings, schools and houses collapsed. Rock falls occurred in the mountains and small cracks on the ground were reported. It was the peak of a seismic crisis with an earthquake swarm centred along the NW–SE trending Chenene Mountains, at about 80 km north of Dodoma. This area is located in a portion of the Eastern Branch of the East African Rift System that has not attracted much attention to earth scientists since the early explorations in the year 1950–1960, especially for the south part of it.

The East African Rift System or EARS (Fig. 1) is the most extensive, currently active zone of continental rifting on the globe (McConnell, 1972; Ebinger, 1989; Delvaux, 1991; Morley, 1999a; Calais et al., 2006). It is often considered as a model for the break-up of continents and the onset of ocean-basin formation (Brown and Girdler, 1980; Chorowicz, 2005). Current volcanism, seismic activity and the presence of hot springs suggest that the rift system is still active (Walker, 1969; Shudofsky et al., 1987; Iranga, 1992; Ring et al., 2005). The East African Rift System has several segments cutting through the continent from the Afar region in Eritrea and Ethiopia down to South Africa (Fig. 1). The well-expressed Eastern Branch traverses Ethiopia (Main Ethiopian Rift), Kenya (Kenya or Gregory Rift) and reaches North Tanzania, where it forms the North Tanzania Divergence. In the region of

Fig. 1. Schematic map of the central part of the East African Rift System (adapted from Delvaux, 1991 and Morley, 1999). Rectangle shows the location of the study area. The border around Tanzania is shown as a light broken line. Bold squares represent Nairobi (N) and Dodoma (D).

Arusha, it splits in three small segments, one running to the southwest (Lake Eyasi), one to the southeast towards the Tanzanian coast (Pangani Rift) and one heading south (Lake Manyara). The latter continues southwards towards Dodoma (Fig. 2), where it is documented by modest fault scarps (up to 200–300 m high), moderately warm thermal springs and surprisingly high seismicity, in contrast with the Kenyan portion of the Eastern Rift, whose rift morphology is much better expressed. Further to the southwest, it finally rejoins the Western Branch in Mbeya region, where it forms a triple junction and gives rise to the Rungwe Volcanic Province (Fig. 1).

This article concentrates on that weakly expressed morphologically but seismically very active, broad, N–S trending rift portion that extends southwards from the North Tanzanian Divergence down to the Dodoma region and makes the link with the Kilombero rift valley to the South (the Manyara–Dodoma Rift segment, Fig. 2). It aims at improving the knowledge about the youngest stage of that

segment by giving new morphostructural, seismotectonic, fault-kinematic and tectonic-stress data in order to better understand the dynamics of rifting in this portion of the East African Rift System.

The recent availability of the 90-m-resolution Shuttle Radar Topography Mission – Digital Elevation Model (SRTM – DEM) data for Africa by spring 2004 changed considerably our view of the topographic expression of rifting, allowing a finer morphological interpretation, with the same level of detail for the entire investigated area. Before the release of the STRM data, morphostructural investigations were based on reconnaissance geological maps, remote sensing imagery (mainly Landsat and Spot), air photography, and, for selected areas, digital elevation models elaborated from the available topographic maps or couples of remote sensing images.

The neotectonic structure of this region is analyzed on the basis of a detailed morphostructural interpretation of the SRTM – DEM, combined with the published
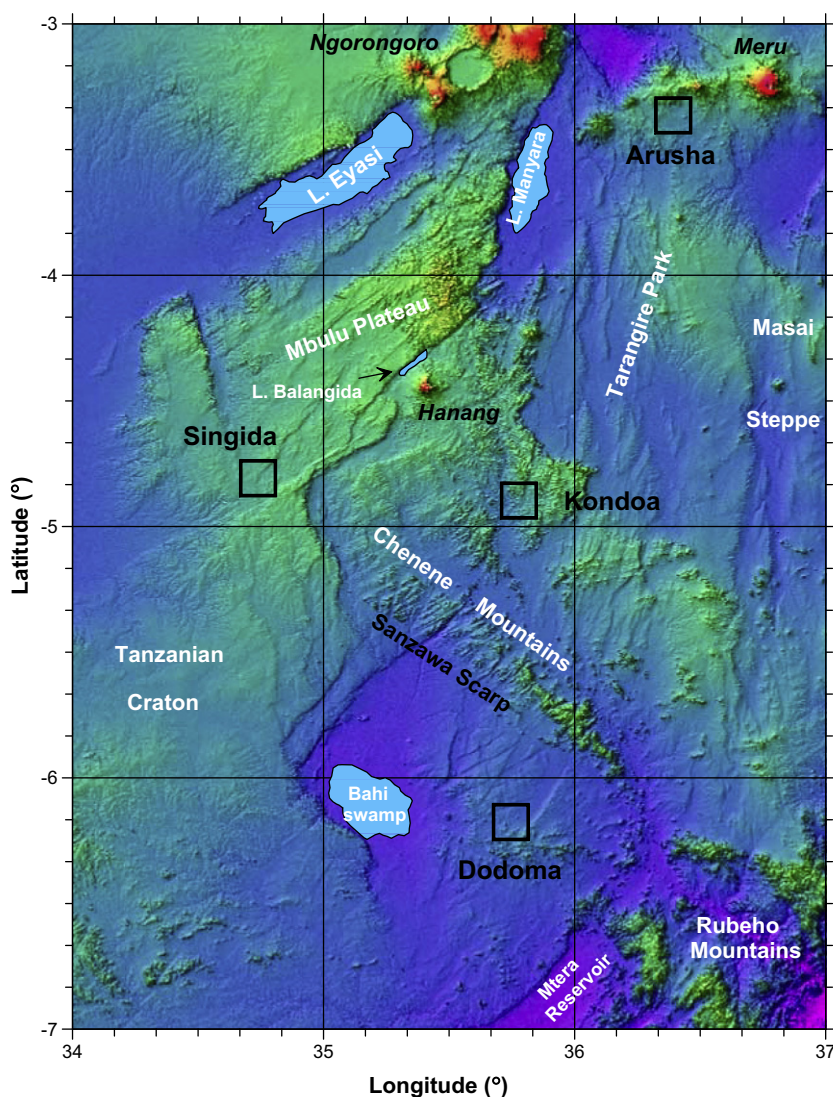

Fig. 2. Grey-coded shaded-relief topography of the Manyara–Dodoma Rift segment in Central Tanzania (Location on Fig. 1). Data are from the 90-m-resolution SRTM. The major towns are labeled in black, and the main physiographic names in white.

1:125,000 geological maps and the available thermal spring data in a Geographic Information System. Field checks in the region surrounding Dodoma supplemented the interpretation. The seismotectonic nature of the Manyara–Dodoma Rift segment is highlighted using recent earthquake seismic epicentre data. The available earthquake focal mechanism data are inverted in order to constrain the present-day regional stress regime. Geological fault and fracture data measured in the field are used to reconstruct the past and recent tectonic stresses. Combining the present regional stress field with the neotectonic fault architecture, slip tendency analysis is applied to further propose an interpretation of the fault kinematics in terms of likelihood of their reactivation.

This paper provides new details on the recent evolution of the North Tanzanian Divergence. It presents the first morphostructural interpretation of the area since the release of the SRTM – DEM data. It shows that the rift is currently propagating southwards of the North Tanzanian Divergence, in a different way that is generally accepted. Implications for seismic risk assessment are also discussed.

2. Geological setting

2.1. Basement structure

The Eastern Branch of the EARS in Central Tanzania (Fig. 1) is located within the Dodoman metamorphic-granitoid Belt. The latter is part of the granitoid Tanzanian shield and was formed by migmatization and then further stabilized by a succession of granitic intrusions (Wades and Oates, 1938; Fozzard, 1962; Barth, 1996).

Whole-rock radiometric dating of the Tanzanian Craton indicates that the ages of the migmatites and granitic complexes of the Dodoman tectonic domain range from 2.5 to 1.87 Ga (Wendt et al., 1972; Gabert, 1973; Gabert and Wendt, 1974; Bell and Dodson, 1981). The Tanzanian Craton (Fig. 1) is surrounded on its southern and eastern sides by the Paleoproterozoic Usagara Belt (Mruma, 1995; Fritz et al., 2005). The northeastern extension of the Usagara Belt is poorly defined as it was reworked into the Pan-African Mozambique Belt (Pinna et al., 2004). Recent zircon age and Sm-Nd whole rock data indicate that Archaean and Paleoproterozoic gneisses dominate in the Mozambique Belt, which were reworked during the Pan-African orogeny (Vogt et al., 2006). The role of the Usagara Belt as to whether it affected or rejuvenated the craton is still under debate (Fritz et al., 2005). The Usagara Belt is thought to have formed by accretion onto the Tanzanian Craton between 2.0 and 1.8 Ga during the collision of an unknown crustal block against the craton with a subduction zone dipping to the west. Deformation occurred in a strike-slip regime, in an island-arc context. The Mozambique Belt was formed by oblique collision between East and West Gondwana with westward thrust propagation during the Pan-African orogeny (650–

580 Ma). Within the Usagaran Belt, the Pan-African overprint occurred in semi-ductile to brittle facies, while east of it, deformation is of lower crustal level in very high grade facies (up to granulite). North of Dodoma, the presence of Usagaran remnants between the Tanzanian Craton and the Mozambique Belt is not clear. Most rift structures are located along the boundary between these two crustal blocks, in the reworked Archaean Dodoman tectonic domain.

Structural geology suggests that the Precambrian structural control on the recent structures associated with the East African Rift System is important in the area (Fairhead and Stuart, 1982).

2.2. The eastern branch of the EARS in Tanzania

The rift structures in North and Central Tanzania (Fig. 1) are commonly described as the southward continuation of the Kenya Rift, traditionally known as the "Gregory Rift". In northern Tanzania (south of Lake Natron), the Eastern Branch of the EARS splits into three separate segments, trending southwest, south and southeast, and forming the North Tanzanian Divergence, (Ebinger et al., 1997; Foster et al., 1997; Foster and Jackson, 1998). The southwestern segment is occupied by Lake Eyasi, and terminates against the Tanzanian Craton. The southeastern segment forms the Pangani Rift and supposedly continues to the Indian Ocean coast. Towards the south, the Gregory Rift extends into the basin of Lake Manyara (Ring et al., 2005) and the rift fades progressively towards Dodoma. Its possible continuation further south is unclear, as it may join the Western Branch of the EARS via the Usangu Depression, forming a triple junction at Mbeya (Delvaux and Hanon, 1993), or even propagate to the system of the Mikumi and Kilombero Depressions superimposed on old Karoo rifts (Le Gall et al., 2004). As opposed to the Western Branch of the EARS, the Eastern Branch is characterized by widespread volcanism, closely related to tectonics (Wilkinson et al., 1986; Dawson, 1992). The Kenyan sector of the Gregory Rift also contrasts strongly with the northern Tanzania sector, in which the tectonically affected area is considerably broader and dominated by basic to ultrabasic magmatism (Dawson, 1992).

As expressed in both volcanic and tectonic activities of the rift faults (timing constrained by dated volcanics and lacustrine sediments), Late Cenozoic rifting in the area occurred in two different stages (legends of the published 1:125,000 geological maps of Tanzania; Wilkinson et al., 1986; Dawson, 1992), corresponding to changes in stress field (Strecker et al., 1990; Bosworth et al., 1992; Mugisha et al., 1997). At around Middle to Late Miocene (ca. 10–12 Ma) the southward-propagating Eastern Branch reached the craton margin (Lubala and Rafoni, 1987; Dawson, 1992; Nyblade and Brazier, 2002) and started to disturb it although the lithosphere of the Tanzanian Craton appears to have remained stable and rigid throughout its

evolutionary history (Weeraratne et al., 2003). At this stage, wide tectonic depressions developed and large amounts of basic magma formed shield volcanoes. In Central Kenya, the stratigraphy of the Miocene volcanic deposits has been refined by Mugisha et al. (1997), based on the new Ar–Ar dating of Deino et al. (1990). A second important phase of faulting is dated between 1.3–1.2 and 0.9 Ma (Fairhead et al., 1972; MacIntyre et al., 1974) and was followed by a period of relatively minor but predominantly explosive volcanic activity, involving nephelinite, phonolite and carbonatite. To our best knowledge, no recent radiometric ages on the rift-related volcanism in the North Tanzanian Divergence are available from the literature. Similarly, a two-stage rifting history is also observed in the Rungwe volcanic region of the Mbeya triple junction between the Eastern and the Western Branches of the EARS (Ebinger et al., 1989; Delvaux et al., 1992; Ring et al., 1992).

The Eastern Branch of the Cenozoic EARS in Kenya and North Tanzania developed mainly within the Mozambique belt, 50–150 km east of the exposed margin of the Tanzanian Craton. It is characterized by a long wavelength Bouguer anomaly with two major components (Nyblade and Pollack, 1992; Tesha et al., 1997). The first component has a signature derived from shallow rift basins and the second component is a short wavelength gravity low attributed to a discrete crustal thickening (2–5 km). The latter is interpreted as forming a crustal root along the suture between the Tanzanian Craton and the Mozambique belt and this suture-thickened crust is proposed to have localized the rifting (Tesha et al., 1997).

In Kenya, the seismic networks operating during the three campaigns of the KRISP project in 1985, 1989–1990 and 1993–1995 showed that the seismicity is higher than previously thought. This motivated the establishment since 1990 of a permanent seismic survey covering the Kenya Rift in the southern half of Kenya. The first results (Hollnack and Stangl, 1998) show that the southern portion of the Kenya Rift, including the North Tanzanian Divergence, displays a significant level of seismicity with more than 2000 recorded earthquakes between October 1993 and August 1996 with local magnitudes up to Ml = 5. A more detailed seismological and neotectonic structural investigation of the Lake Magadi area in South Kenya (just north of Lake Natron, Fig. 1), supported by a dense network of 15 seismological stations took place between November 1997 and June 1998 (Ibs-von Seht et al., 2001; Atmaoui and Hollnack, 2003). They confirm that the Lake Magadi area is seismically active and with recent (younger than 5000 years old) tectonic activity related to ongoing rifting. This Quaternary rift activity is mainly concentrated in the axial zone of the rift, as shown by seismically induced open fissures and non-seismic joints. Studying neotectonic joints and open fractures at different scales, Atmaoui and Hollnack (2003) defined a N105°E (WNW–ESE) regional extension direction.

3. The Manyara–Dodoma Rift segment

In many syntheses on the EARS, the role of the North Tanzanian Divergence in the southward propagation of the Eastern Branch into Tanzania is highlighted (e.g. Foster et al., 1997; Chorowicz, 2005) but the neotectonic importance of the rift structures south of lakes Manyara and Balangida (Fig. 2) is often underestimated. It is known however that current seismic and neotectonic activity continues southwards to Dodoma and even to the Mikumi–Kilombero Rift (Nyblade and Brazier, 2002; Le Gall et al., 2004). The rift structures forming the southwards continuation of the Gregory Rift valley in Central Tanzania have been mapped in relative detail in the published 1:125,000 geological maps of Tanzania. James (1967a), in his compilation of the thermal springs of Tanzania, presents a synthetic map in which the formation of this part of the rift is explained by "block-faulting and tilting" in what would now be described in a half-graben geometry. James (1967a) already recognized that the major border fault is systematically on the western side of the basins ("inland drainage basins"), globally N–S trending but in a zig-zag way. It defines successively the Natron, Manyara and Bahi asymmetric inland drainage basins, occupied by their respective lake or swamp (Fig. 2). On the geological maps, it also appears that recent faulting occurs in a broad zone of crustal deformation extending north–south from lakes Eyasi and Manyara to the Mtera dam reservoir, between the Tanzanian Craton on the west and the Masai Steppe on the east (Fig. 2). This justifies the choice of the study area, between the Ngorongoro and Meru volcanoes to the north, the Mtera dam reservoir and Rubeho Mountains to the south.

The main physiographic elements of the northern part of the study area, near Arusha, comprise the wide rift depressions of lakes Eyasi and Manyara and the large volcanoes of Ngorongoro and Meru (Fig. 2). The relatively low land to the northeast is formed by the Manyara Depression (960 m a.s.l.), the Tarangire Park and the Masai Steppe (1200–1400 m a.s.l.). Both are separated from the Bahi Depression (940 m a.s.l.) near Dodoma by NW–SE trending highlands between Singida and Kondoa forming the Mbulu Plateau (up to 2420 m a.s.l.) and the Chenene Mountains (up to 2060 m a.s.l.). The 3417-m-high Hanang volcano, a young nephelinitic eruptive centre corresponds to the second rift stage and forms the southernmost Neogene volcanic centre in the Eastern Branch (Thomas, 1963; Dawson, 1992). Further south, after the Fufu Fault, the depression in which the Great Ruaha River flowed is now dammed, forming the Mtera reservoir (Fig. 2). To the extreme southeast of the study area, the Rubeho Mountains (up to 2300 m a.s.l.) form the rift shoulder of the Mikumi Depression.

Covering a large part of the Dodoman rocks in this area, the Kilimatinde Cement consists predominantly of silcrete (silicified sandstone), but locally also of calcrete or ferricrete. Fozzard (1961) considers the Kilimatinde Cement

to have formed in shallow evaporative basins developed on a quasi-planar land surface, between residual hills. Where eroded down to the weathered basement, the Kilimatinde Cement shows a thickness of 15–30 m. In the Bahi Depression, the Kilimatinde Cement is overlain by about 75 m of lacustrine sediments of possible Plio-Pleistocene age made of calcareous and/or siliceous or alkaline clays, rich in brines (Fawley, 1956). The Kilimatinde Cement may be as old as Miocene to Early Pliocene, but this age estimate needs to be confirmed. The Kilimatinde Cement is found in the Bahi Depression and NW of it, but its extent is limited to the NE by the Sanzawa Scarp (Fig. 2). This suggests that the Chenene Mountains were already hanging over the depositional area of the Kilimatinde Cement, acting as the source of sediments and separated from it by the Sanzawa Fault, which was therefore active during deposition. All faults surrounding the Bahi Depression, except the Sanzawa Fault, displace the Kilimatinde Cement and are therefore related to a younger rift stage.

The Dodoman basement is largely outcropping in the Mbulu Plateau and the Chenene Mountains (Fig. 2). The basement of the latter is known as the Kwa-Mtoro block. Numerous dolerite dykes, consistently trending NE–SW are present in these two basement outcrops (1:125,000 geological maps: QDS 68 Lake Eyasi, 84 Hanang and 123 Kwa-Mtoro). They are assumed by Thomas (1963) to be of Bukoban age (Late Neoproterozoic, Early Cambrian). In the Kwa-Mtoro block, ENE–WSW trending cataclasites and brittle-ductile shear zones are also present. This trend is parallel to the Sanzawa Fault which probably reactivates a basement shear zone (Fozzard, 1961).

The region of investigation has a complex network of tectonic structures, most of which are Precambrian in origin. The recent structures associated with the rift system are locally well expressed, often reactivating Precambrian discontinuities (Fairhead and Stuart, 1982). Between Dodoma, Singida and Kondoa, the dominant trend of the Dodoman tectonic domain is WNW–ESE with some fluctuations, best expressed in quartzitic rocks. Superposed to it is a NE–SW trend of brittle-ductile structures that are well expressed on the landscape and that could possibly be related to the Pan-African orogeny (by comparing with Fritz et al., 2005).

4. Analysis of tectonic stress

The key task in tectonic stress field analysis of geological fault-slip data or earthquake focal mechanisms entails reconstruction of a reduced stress tensor which best models the state of stress of the given volume of rock sampled at outcrop scale for fault-slip data or at regional scale for focal mechanisms (Angelier, 1989, 1994; Delvaux and Sperner, 2003).

Out of the six independent variables from the complete stress tensor, four can be determined by inverting fault-slip or earthquake focal mechanism data alone and constitute the "reduced stress tensor" (Angelier, 1989, 1994): the ori-

entation of the three orthogonal principal stress axes: σ_1, σ_2 and σ_3, where $\sigma_1 \geqslant \sigma_2 \geqslant \sigma_3$ and the "Stress Ratio" $R = \sigma_2 - \sigma_3 / \sigma_1 - \sigma_3$, which expresses the magnitude of σ_2 relative to the magnitudes of σ_1 and σ_3. The basis of the stress inversion techniques has been described elsewhere (Wallace, 1951; Bott, 1959; Angelier, 1989).

The tectonic regime is expressed by a "Stress Regime Index" (R') defined from a combination of the Stress Ratio (R) and the nature of the most vertical stress axis (as in Delvaux et al., 1997; Delvaux and Sperner, 2003). R' is defined in order to express the stress regime on a continuous scale from 0 (radial extension) to 3 (constriction) and ranges from 0 to 1 for normal faulting regimes (σ_1 sub-vertical), from 1 to 2 for strike-slip regimes (σ_2 sub-vertical) and from 2 to 3 for thrust faulting regimes (σ_3 sub-vertical).

4.1. Fault-slip data

From each site, brittle structural data (fault-slip data) are measured along exposed fault scarps and on faults and fractures in rock outcrops. They include fault planes with slip lines (slickensides) and indication of slip sense (e.g. Petit, 1987; Angelier, 1989), and also other small-scale brittle microstructures, such as shear or tension joints (e.g. Dunne and Hancock, 1994; Delvaux and Sperner, 2003). In the field, the quality of slip sense or joint type determination is evaluated as Certain, Probable, Supposed or Unknown.

In order to separate the slip data into different subsets, other important observations are made in the field: (a) type and degree of mineralization or material found on the fault planes, (b) the presence or absence of fault gauges, (c) cross-cutting relationships... The significance of the stress tensors determined on these subsets is interpreted in terms of tectonic stages and assigned preliminary relative age estimation.

4.2. Qualitative classification of fault surfaces

According to the type of fault rock within a fault zone (fault gauge development, cataclastic/mylonitic fabric, type of mineralization...), it is possible to estimate on a relative basis the paleo-depth at which faulting occurred. Faults that occur deep in the crust (including shear zones) are usually associated with mineralization or at least with alteration minerals, such are chlorite, and epidote (McClay, 1987). Faults associated with Fe-oxides such as haematite on their surfaces are formed closer to the surface in an oxidizing environment. Barren fault surfaces are also common in this environment. The presence of clay gauges indicates that faulting occurred in subsurface conditions with clay percolating from the superficial soil into the voids left in the fault plane during movement(s). This variation with depth of the type of fault rock in a fault zone can be in a simple approximation used as a proxy for the relative timing of faulting, taking into account the time needed to

exhume the fault rock from the depth of formation to the subsurface where it has been observed. Within this logic, the fault rock as seen at outcrop can be considered on a relative time scale as the youngest when characterized by fault gouge, older with slip surfaces coated by Fe-oxides and the oldest when it consists of cataclasite affected by chlorite–epidote metasomatism.

4.3. Paleostress inversion and quality ranking

Data processing for paleostress inversion was done using the new Win-Tensor program, the Windows version of the TENSOR program developed by D. Delvaux, according to the procedure described in Delvaux and Sperner (2003) and using Quality Ranking scheme as in the World Stress Map project (Sperner et al., 2003). The data were processed interactively, first using the "Right Dihedron Method", a graphical method for determination of the range of possible orientations of σ_1 and σ_3, and then using the "Rotation Optimization Method", using the misfit *function F5* of Delvaux and Sperner (2003). This function takes into account not only the angular deviation between the observed slip lines and the modeled shear on every plane using the stress tensor that is being tested, but also the normal and shear stress magnitudess. The quality ranking of the stress tensor obtained (A: excellent, B: good, C: medium, D: poor, E: to be rejected) is based on a series of parameters including: (1) the number of fault data used in the stress determination (n); (2) the proportion of data used relative to the total data set (n/nt); (3) the confidence level in determination of the slip sense for faults (or fracture type for fractures) and (4) the type of fault data used.

5. Neotectonic structure

5.1. Analysis of the SRTM – DEM and neotectonic map

The recent availability of the SRTM digital topographic data at 90 m resolution (released in spring 2004 for Africa) gives new insights with unprecedented detail in the morphology associated with rifting. Before the release of the SRTM data, it was difficult to obtain relief data with an appropriate resolution for evidencing neotectonic fault scarps of a few meters to a few tens of meters high. One solution was to digitize the contour levels of the 1:50,000 topographic maps, as was done for the Rukwa–Tanganyika link in the Western Branch (Fernandez-Alonso et al., 2001). However, this technique was not applicable for the Eastern Branch of the EARS as the coverage of topographic maps is heterogeneous in quality and some of them are quite old. Neotectonic fault scarps were already indicated on the 1:125,000 geological maps, but the map coverage is restricted to the axial part of the rift and is far from complete. Other techniques for producing detailed DEM for small areas involve the processing of couples of remote sensing images.

Traditional remote-sensing images are often used to obtain a more detailed and homogenous image of the rift morphostructures, but their resolution does not allow deciphering the active fault scarps a few meters to tens of meter high. This partly explains why the recent rift structures in the region of Dodoma have been under evaluated.

The new STRM-derived DEM was taken as a basis for the interpretation of the recent tectonic structures of the Eastern Branch of the EARS in Central Tanzania. The SRTM – DEM data were processed in order to produce colour-coded elevation maps with artificial shading. Following a preliminary interpretation, a field campaign was organized to examine in situ the tectonic morphostructure, to detail the major and minor fault scarps, to perform a structural analysis at the outcrop scale, to dig preliminary paleoseismic trenches and to record the location and setting of thermal springs. After the fieldwork, the DEM data were re-interpreted and morphostructural data compiled with support of the existing geological maps.

The data on recent faults, thermal springs and the major volcanic centres are compiled on a neotectonic map (Fig. 3). Faults that display a fresh morphology of their associated scarp are considered to have been active in the Quaternary and are consequently interpreted as recent. The major volcanic centres, with the nephelinitic Hanang volcano, the explosive Meru volcano and other centres in the area of lakes Manyara and Eyasi, generally belong to the second rift stage, which started at around 1.2 Ma. The data on thermal springs come from the compilation of James (1967a), Walker (1969), additional descriptions of Hochstein et al. (2000), the available 1:125,000 geological maps and our own observations in the Gonga spring field near the Bubu Fault and the Manyeghi helium spring field along the Mponde Fault. They are detailed hereafter.

5.2. Thermal spring data

Thermal springs are known to be frequent in the EARS. They are also known since long times by local people. The most important ones are reported on the geological maps and even on the topographic maps, sometimes reflected in the local names. They have attracted a particular attention as they can be the source for commercial salt deposits and noble gases. In Tanzania in general and in the study area in particular, a large number of thermal springs are known and some of them have been studied in relative detail between 1950 and 1962 by the Geological Survey of Tanganyika. After the discovery in 1947 of helium, argon and nitrogen in the gas emitted by the Nyanza cold brine spring at Uvinza (W-Tanzania), intensive investigations were carried out by the East African Office of the UK Atomic Energy Authority in 1957 and 1958 for evaluating the potential of some spring as a source of helium. The main localities explored were the Maji Moto field (near Musuma, Lake Victoria in N-Tanzania) and the Manyeghi helium springs along the Mponde fault within the study area (James, 1967a). They belong to a group of thermal
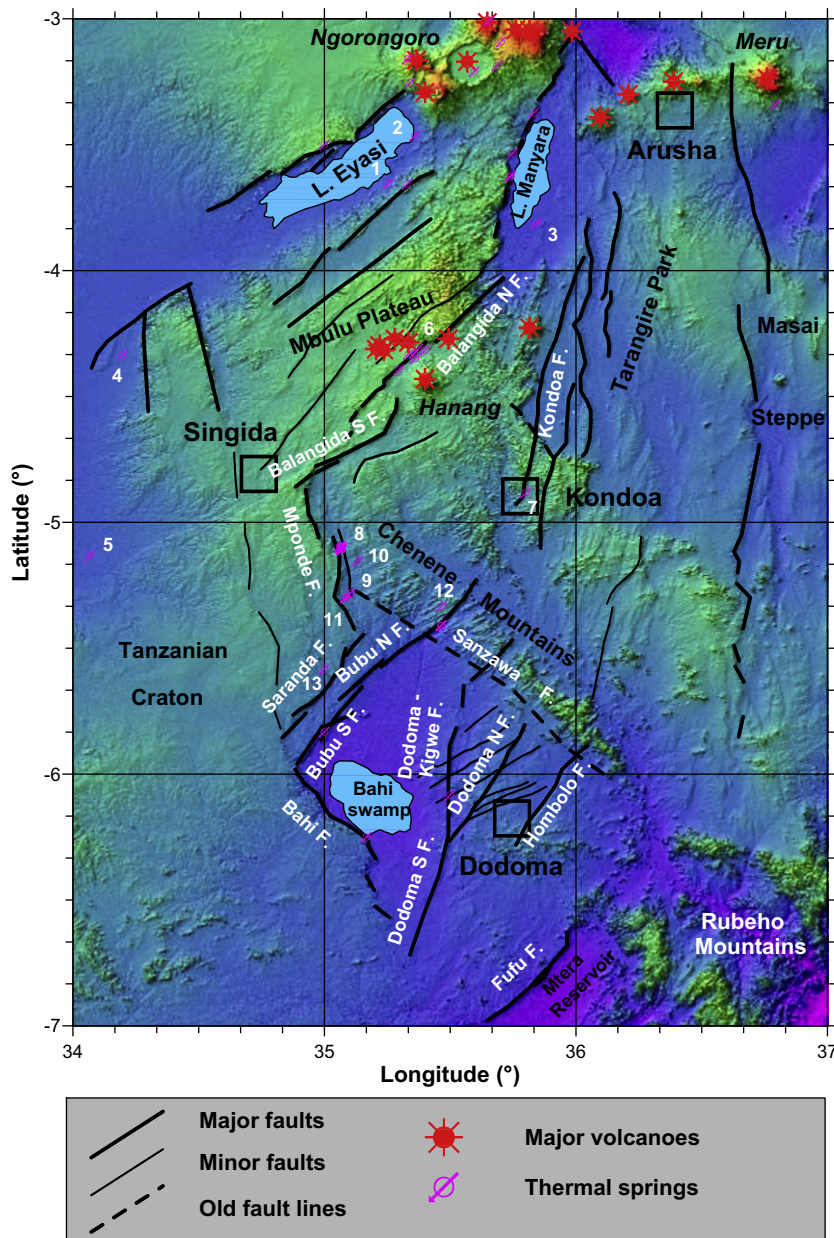
Fig. 3. Neotectonic structure of the Manyara–Dodoma Rift segment in Central Tanzania shown on the SRTM topography as in Fig. 2. In addition to the major towns (in black) and the main physiographic names (in white), the name of the major faults discussed in the text are also shown. All features displayed (faults, volcanic centres and thermal springs) belong to the most recent rift stage that initiated 1.2–1.3 Ma ago and that is still active. The physical and chemical data from the thermal springs numbered 1–13 are reported in Table 1.

springs with Na, K dominated salts in brines and helium-argon-nitrogen bearing gases.

Table 1 gives a synthesis of the available physical and chemical data compiled from the work of James, Harris and Walker. Since the 1957–1958 campaign, no major additional analytical work has been done on these springs. No isotopic data are available for the Manyeghi helium springs, but some are reported by Morgan (in James, 1967b) for the Maji Moto springs near Musoma, outside the study area. At the Maji Moto site, the $^{40}Ar:^{36}Ar$ isotopic ratio amounts to about 800:1 in the spring gases while it is about 300:1 in the air. Conversely, the measured $^{14}N:^{15}N$

ratio in the spring gas (270:1) is similar as for atmospheric nitrogen. Morgan concluded that nitrogen in the spring gases is of atmospheric origin, and that the argon and helium have been added in a substantial way from a juvenile source, probably of radiogenic origin. He suggests that argon and helium have their source deep in the crust, channeled to the surface by old shear zones. Similarly, Arad and Morton (1969) also consider that in the thermal springs of the Western rift Branch in Uganda, most of the solutes are from juvenile source while the water is probably meteoric.

In the Manyara–Dodoma area, many of the springs with nitrogen/helium occur in an arid environment and

Table 1
Physical parameters and chemical composition of gas and water from the major thermal sites

Springs													
Spring name	Eyasi	Eyasi	Kinyoo	Itebu	Isanza	Golai	Kondoa	Manyeghi	Sumbaru	Takwa	Mponde	Gonga	Hika
Spring number	1	2	3	4	5	6	7	8	9	10	11	12	13
Fault structure	Eyasi	Eyasi	Manyara			Balangida	Kondoa	Mponde	Mponde	Mponde	Mponde	Bubu	Saranda
Location													
Latitude (°)	−3.654	−3.4637	−3.812	−4.333	−5.133	−4.312	−4.883	−5.100	−5.282	−5.152	−5.300	−5.333	−5.583
Longitude (°)	35.255	35.361	35.845	34.200	34.067	35.372	35.800	35.064	35.103	35.134	35.083	35.467	35.000
Physical properties													
Temperature (°C)	−	35	25	22		30	31	33.1 ± 4.9		38	42	47	28
Water flow (l/h)	−	Small	Small	3300		110	90,800	227,000				6800	8200
Gas flow (l/h)	−	Small	Small			Small	100	3650		100	200	15	5
Gas analysis (vol%)													
CO_2	0.2	8.2	0.7	4.2		3.8	3.9	1.1 ± 0.4		1.6	0.2	1.4	0.6
H_2S	<0.1	1.0	0.2	0.4		0.8		0.1 ± 0.2		0.9	Trace	0.5	Trace
CO	<0.1	0.2	1.1	0.1								0.4	0.2
O_2	0.8	0.3	0.4	0.4		0.4	2.7	0.1 ± 0.1		0.1	0.2	n.d.	n.d.
H_2	0.2							0.2 ± 0.3		0.5		n.d.	n.d.
CH_4	<0.1	80.3	88.5	1.6				0.2 ± 0.1		1.1	0.4	1.4	2.9
He	5.7		0.07	0.74		3.7	0.3	5.4 ± 0.7		7.0	10.2	7.7	7.1
Ar				1.02			1.0	1.5 ± 0.1		1.3	1.5		
N_2	93.1	10.0	9.0	91.6		91.3	91.6	91.5 ± 1.2		87.5	87.5	88.8	89.2
Water analysis (ppm)													
NaCl	8490		2965	26	643	4320	193	1434 ± 152	1250	1010	1,189	211	89
Na_2CO_3	1730		8510			1900		76 ± 50		27	48		
$NaHCO_3$	4630			396	215	2450		764 ± 79	328	277	264	160	150
Na_2SO_4	1000			30	231	1690	58	643 ± 151	544	649	530	220	49
NaF	150			2	17	78	2	24 ± 3	19	9	24	11	11
KCl						142		18 ± 2		15	11		
$Ca(HCO_3)_2$				89	32		248	39 ± 8	24	88	20	218	52
$Mg(HCO_3)_2$				151	30		183	14 ± 6		24		24	5
SiO_2			110				60					50	50
pH	9.5			7.5	8.5		7.5	8.5 ± 0.3	8	8.5	9.5	6.9	8.1

Compilation from James (1957, 1958, 1967a), Harris (1958, 1959) and Walker (1969). The springs are located on Fig. 3 using their spring number.

are situated in crystalline basement rocks with little or no sedimentary cover. They are also relatively far from centres of volcanic activity. Most of them are connected with major fault lines, inferred to penetrate deeply in the crust. Sometimes, they are indirectly related to major rift faults by means of antithetical faults as in the Manyeghi helium spring field (geology detailed by Fozzard, 1959). In conclusion of his review, James (1967a) favours a mixed meteoric and juvenile source for the thermal springs. He further suggests that the juvenile could be volatile components emanating from the mantle, rather than from magmatic bodies.

5.3. Morphostructural interpretation

On the SRTM – DEM (Fig. 3), a persistent NW–SE basement tectonic grain is well expressed in the morphology of the uplifted basement blocks. This trend does not correspond to the mapped ductile structures of the Dodoman basement, but rather to a series of dolerite dykes and associated brittle to semi-brittle dislocations that affect the pre-existing ductile structures. These structures are not constrained in age, but they could represent the late stages of the Pan-African orogeny. They obviously control the trend of most neotectonic rift faults.

The largest tectonic scarps bordering lakes Manyara and Eyasi on their western or northwestern side are likely inherited from the Late Miocene to Pliocene rifting stage (Dawson, 1992). They trend NNE for the Manyara fault scarp and NE for the Eyasi fault scarp. In contrast, the NW-trending Sanzawa fault scarp that separates the Bahi Depression (Bahi Swamp on Fig. 3) from the Chenene Mountains does not seem to have been reactivated in recent times. It appears much degraded (less morphologically fresh) than the other scarps.

Recent faults guided by the basement tectonic grain cut across the exposed basement blocks (Chenene Mountains and Mbulu Plateau). They seem to propagate from the earliest fault scarp, inherited from the first rifting stage, linking together different segments that probably developed independently. Together, they form a zig-zag network with two dominant trends: NE to ENE, NNW, and an apparently new N–S trend, still weakly expressed and incompletely developed.

Connected to the Manyara fault scarp, a set of discrete but morphologically fresh fault scarps cross-cut the Mbulu Plateau in a NE direction, roughly parallel to the trend of the diabase dyke swarm. They displace the superficial Pio-Quaternary deposits and are associated with recent volcanic explosive craters (i.e., the Hanang volcano and satellites) and hot springs. They all have the downthrown block on their south eastern side. The most important of these faults is the Balangida Fault, determining the extent of Lake Balangida and the presence of warm, salty springs with gas at the foot of the rift scarp. In particular, Lake Balangida develops in the relay zone between two segments of the Balangida fault system (Fig. 3).

More to the south, SW-trending faults also exist in the Bahi Depression and surroundings, the most prominent being the Saranda, Bubu, Dodoma, Hombolo and Fufu Faults. Except for the antithetic Hombolo Fault, they all have their southeastern block down-thrown. Inside the Bahi Depression, there are also some minor faults. Some of the faults, like the Bubu and the Hombolo Faults, cross-cut the Sanzawa line and partly affect the Chenene Mountains, in a direction parallel to the NE–SW tectonic grain of the basement. He-bearing, moderately warm springs are known along the Bubu Fault, in particular where it crosses the Chenene Mountains (i.e., at the Gonga thermal spring field).

At a high angle to the preceding trend, NNW-trending faults are less abundant, but equally well developed. The Mponde Fault, linking the NE-trending Balangida South and Saranda Faults, controls the formation of a small graben. The main Monde Fault dips to the east and a minor antithetic fault controls the location of He-bearing, moderately warm springs. Another east-dipping, NNW-trending fault system limits the Bahi Depression from the flat morphology of the Tanzanian Craton and possibly continues towards Singida, up to the western part of the Eyasi Rift valley.

In addition to the two preceding fault trends that define lozenge-shaped blocks in a zig-zag pattern, a system of N- to slightly NNE-trending and relatively weakly expressed faults is also present. It extends from north of Arusha and the Tarangire Park, down to Kondoa and it is also present in the Bahi Depression near Dodoma. The northern extremity of the Bubu Fault also rotates from a general NE-trend into a NNE-trend, in the same alignment as for the Kondoa Fault. Both faults have hot springs along them.

The presence of recent volcanic centres of the second rifting stage and thermal springs along the three fault systems (NE-, NNW- and N-trending) suggest that these faults belong to the recent rifting stage and are tectonically active.

6. Seismotectonic pattern

6.1. Seismic catalogues

The distribution of seismic epicentres is examined on the basis of two different sources of data: (i) an international seismic catalogue recorded during the instrumental period (for Africa) between early 1921 and late 2006, and (ii) the catalogue of earthquakes recorded during 1994–1995 by the Tanzania Broadband Seismic Experiment. The international seismic catalogue is compiled from USGS data and contains 122 teleseismic earthquakes with magnitudes Mb ranging from 3.5 to 6.2. The strongest of these events occurred in April 16, 1922 but is poorly located.

In October 1997, R.A. Brazier compiled a regional catalogue using data from the 1994–1995 Tanzania Broadband Seismic Experiment Project (Nyblade et al., 1996). For the region between 3–7°S and 34–37°E, this catalogue

contains 1395 earthquakes with epicentre locations and magnitudes Mb (when determined) ranging from 0.8 to 5.9. These were recorded between May 1994 and May 1995, with the strongest earthquake in December 23, 1994.

6.2. Distribution of seismic epicentres

The Manyara–Dodoma Rift segment is shown to be seismically active on the maps compiled by Fairhead and Girdler (1972) and Morley (1999b). However, its high level of microseismicity was only revealed after the establishment of local and temporary dense seismic network (Nyblade et al., 1996; Hollnack and Stangl, 1998).

The compiled international catalogue from teleseismic earthquakes (1921–2006) contains less numerous data (112) but with relatively higher magnitudes (Mb: 3.5–6.2) compared to those from the Tanzania Broadband Seismic Experiment catalogue. The former are mainly teleseismic earthquakes recorded by the world regional seismic network. These earthquakes are distributed along a broad N–S belt, mainly between 35°E and 36°E, between the Ngorongoro crater, Arusha, Singida and Dodoma. This seismically active zone corresponds to the region characterized by the highest concentration of young fault scarps as seen on the SRTM – DEM (Fig. 4). An alignment of earthquake epicentres is noticed along the NW–SE trending
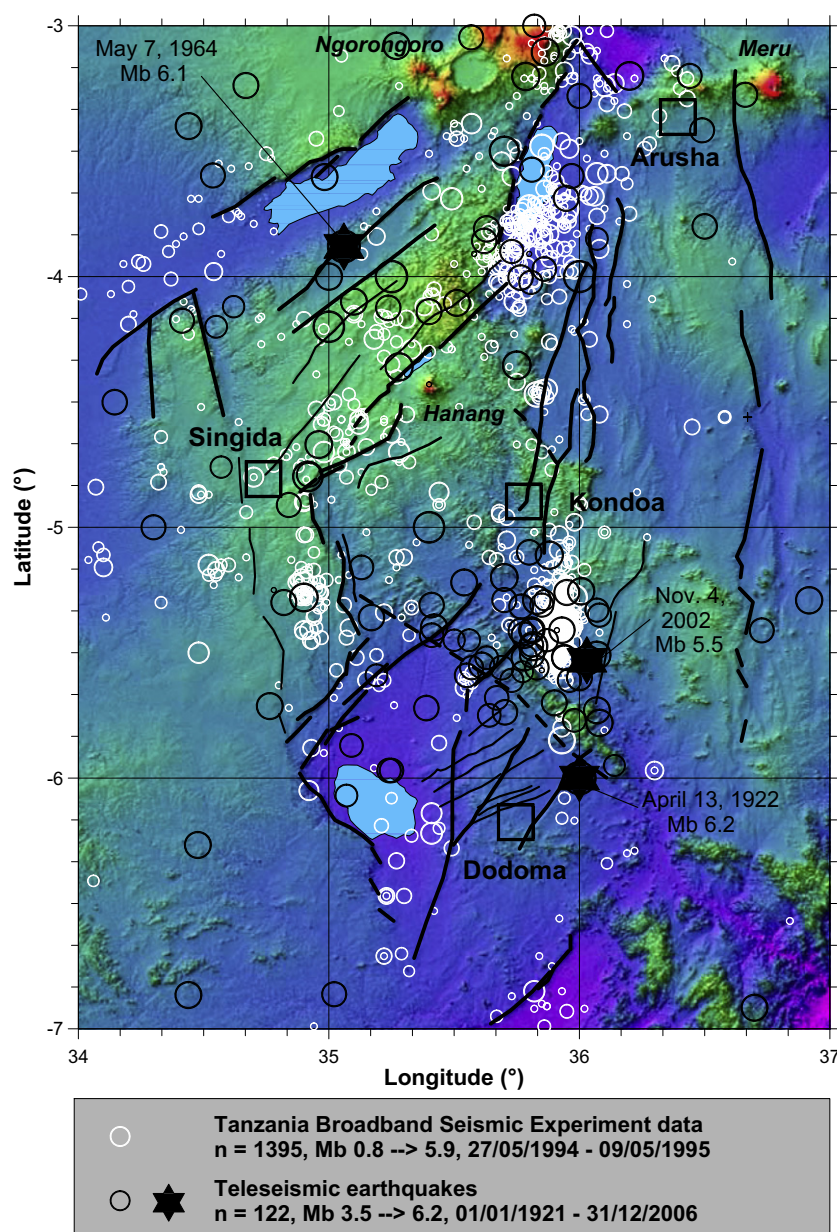

Fig. 4. Seismic epicentre map of the Manyara–Dodoma Rift segment in Central Tanzania shown on the SRTM topography as in Fig. 2. Data are from the Tanzania Broadband Seismic Experiment (Courtesy to A. Nyblade, white circles) and from the USGS (teleseismic earthquakes, black circles). Large black stars show the location of the major earthquakes. The Tanzania Broadband Seismic Experiment data are clustered around several earthquake swarms, one at the southern extremity of the Manyara graben and one in the Chenene Mountains.

Sanzawa Fault and a marked concentration of epicentres occurs in the Chenene Mountains, in relation to the aftershocks of the November 4, 2002 Mb 5.5 earthquake (Fig. 5). It is also close to the poorly located April 16, 1922 Mb 6.2 event, at the junction between the Hombolo fault and the Sanzawa scarp.

The Tanzania Broadband Seismic Experiment catalogue is limited to about one year of measurement (1994–1995) and contains a large number of data (1395 for the study area) of relatively small magnitude (Mb: 0.8–5.9), many of which cannot be detected by the international network (Fig. 4). The configuration of the temporary network centred on the Tanzanian Craton ensures a homogeneous spatial coverage within the studied region. The distribution of epicentres from this catalogue reinforces the trend shown by the data of the international catalogue. Epicentres cluster in several nodes of high epicentre concentration. One of them is located immediately south of the Manyara Depres-

sion, in an area of fault interaction between Lake Manyara and the Hanang Volcano. Another node with a high concentration of earthquakes forms an elongated N–S swarm in the Chenene Mountains, in the same area where the 2002–2003 earthquake swarm later developed. The December 23, 1994 Mb 5.9 event was the strongest of the 1994–1995 swarm.

A smaller earthquake swarm, also N–S elongated, is seen a few km west of the Mponde Fault, in a block bounded by N–S faults, south of Singida.

6.3. Macroseismic evidence

Earthquake shaking has regularly been reported by local people, sometimes with significant macroseismic effect. In addition to the November 4, 2002 Mb 5.5 earthquake in the Chenene Mountains, the May 7, 1964 Mb 6.1 earthquake which occurred along the southern border of the
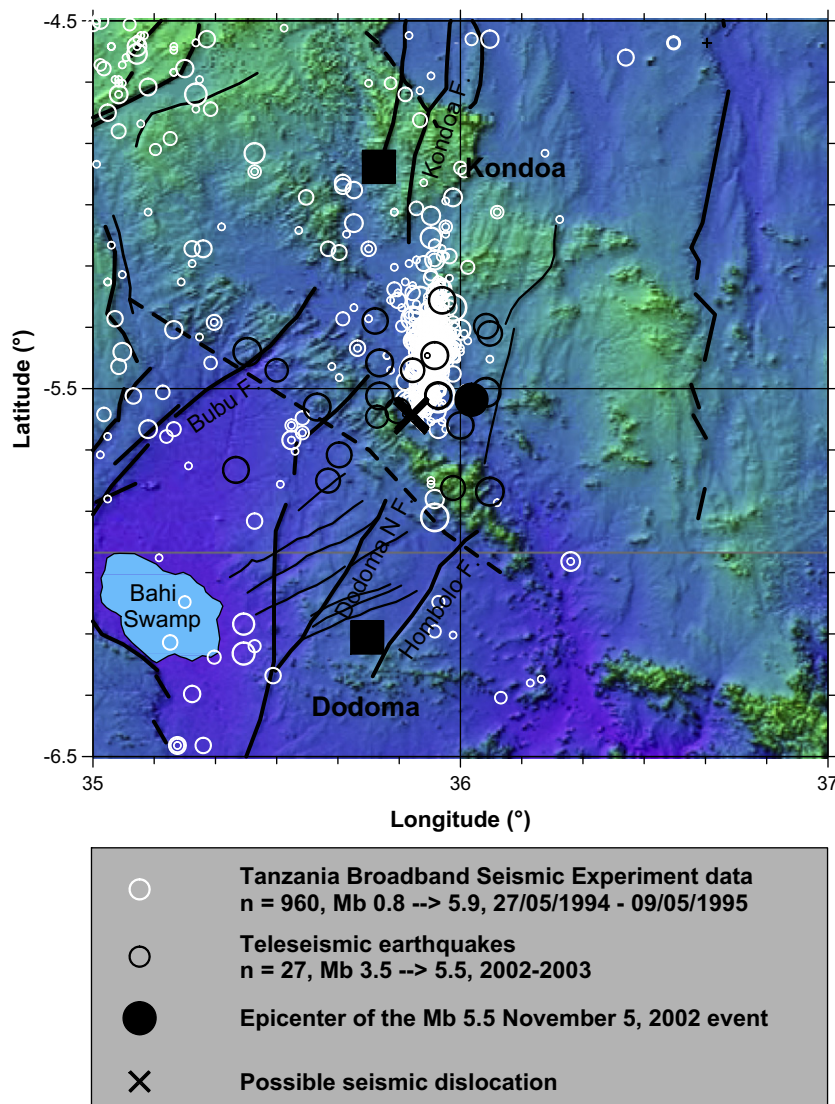

Fig. 5. Detail of the neotectonic structure with the seismic epicentres for the Chenene Mountains. It shows that the Chenene Mountains are actively deforming between Kondoa and Dodoma. The N–S faults near Dodoma and Kondoa apparently tend to propagate towards each other, initiating a new N–S fault across the Chenene Mountains that is not yet expressed at the surface except by some few possible seismic dislocations.

Eyasi basin was also strongly felt (Fig. 4). No other details are available so far. An "earthquake fountain" (mud volcano) in the Surea district (north of Kondoa) was reported to be associated with that event (Selby and Mudd, 1965). In the field, at Gonga village along the Bubu Fault, an old man reported to have felt a strong earthquake in 1964. That earthquake has been reported to have killed four and injured 500 persons.

Surface dislocations in the form of open aseismic fractures are reported by local villagers in their fields, in the Chenene Mountains close to the Great North Road and near Chenene village (Fig. 5). Following the villagers report, the fractures appeared in February 2004. If they are correct about the year of appearance, these fractures are not associated with known earthquakes, as no earthquakes are reported in the international catalogue for 2005 in the Dodoma region. Within a window of 2–3 years, the strongest events were recorded in November 4, 2002 (Mb 5.5; the one that hit the Parliament), June 14, 2003 (Mb 5.1) and December 07, 2003 (Mb 4.9). All of them are of relatively moderate intensity. The fractures are a few meters long and of various orientation, but they occur along a NNE-trending line. This system of cracks occur in an area where no neotectonic fault scarps have been mapped, but they lie in the alignment between the NNE-trending Dodoma North fault, and the N–S trending Kondoa fault system (Fig. 5). It is also located close to the epicentre of the November 4, 2002 Mb 5.5 earthquake, and at the southern extremity of the 1994–1995 earthquake swarm recorded by the Tanzania Broadband Seismic Experiment. More detailed work on these dislocations is under way.

7. Present stress from earthquake focal mechanisms

The most commonly used stress indicators employed to image present-day tectonic stress in the World Stress Map are earthquake focal mechanisms (Zoback, 1992; Sperner et al., 2003). From the North Tanzanian Divergence to

Dodoma, only 12 earthquake focal mechanisms are available. They come from different sources: seven from the Harvard Centroid Moment Tensor catalogue, two from Kebede and Kulhanek (1991) and four from smaller earthquakes recorded by the Tanzania Broadband Seismic Experiment (Brazier et al., 2005). Two different solutions of the same event (i.e., December 15, 1977) are included in the database used in stress inversion (one from the Harvard catalogue and one from Kebede and Kulhanek, 1991) as it was not possible to determine *a priori* the solution to be favoured (Table 2a).

For the focal mechanisms in the World Stress Map, the kinematic p-, b- and t-axes are used to infer the orientations of the horizontal principal stress axes, SH_{max} and Sh_{min} (Zoback, 1992). Strictly speaking, the kinematic p-, b- and t-axes represent strain axes, and not stress directions. However, statistically, by averaging a great number of data (e.g., focal mechanism data, that can represent 2/3 of the data in the World Stress Map), the stress trajectories are considered to be accurately determined by the kinematic axes. Here, as the small number of data does not allow this approach, a full stress inversion has been performed on the 13 available focal mechanisms (indexed 1–13 in Table 2a), representing 12 different earthquakes. These are plotted on Fig. 6 as beach balls and with their Sh_{min} direction and stress regime on the map.

The inversion is performed using the new WinTensor program with the procedure developed for the inversion of focal mechanism data described in Delvaux and Sperner (2003) and briefly highlighted above for geological fault slip data. In the course of the interactive tensor inversion and data separation, 10 data out of the initial 13 were selected (i.e., nr. 1, 2, 3, 4, 5, 7, 8, 9, 12, 13), on which a pure normal faulting stress tensor was obtained with a ENE–WSW horizontal principal extension ($Sh_{min} = N80°E$), a stress ratio $R = 0.5$ and a C (medium) quality (Table 2b, Fig. 7a and b). The limiting factor for the quality estimation is the number of data retained in the

Table 2a
Focal mechanism data displayed on Fig. 6 and used in the stress inversion as displayed in Fig. 7a

	Date	Time	Lat (°)	Long (°)	Mb	Source	Strike	Dip	Slip	SH_{max}	Sh_{min}	Reg.
1	19720213	10:02:00	−4.50	34.10	5.0	Kebede	340	62	−061	146	56	NF
2	19771215	23:20:04	−4.80	34.92	5.6	Harvard	151	31	−064	128	38	NF
3	19771215	23:20:04	−4.80	34.90	12.0	Kebede	348	56	−129	12	102	NF
4	19900405	19:20:48	−3.05	36.05	5.1	Harvard	352	45	−090	172	82	NF
5	19900515	15:21:28	−3.43	35.77	4.7	Harvard	332	29	−106	166	76	NF
6	19900515	16:24:25	−3.12	35.40	5.2	Harvard	059	43	−136	96	6	NF
7	19910222	22:06:01	−3.94	35.94	4.4	Harvard	182	45	−104	12	102	NF
8	19940129	00:23:33	−5.03	35.92	4.1	Brazier	162	43	−71	148	58	NF
9	19940212	16:37:33	−3.88	35.67	4.5	Brazier	316	68	−77	131	41	NF
10	19940720	11:32:03	−4.25	35.58	4.5	Brazier	301	64	−11	76	166	SS
11	19941127	04:20:53	−4.08	35.83	4.0	Brazier	93	69	−22	52	142	SS
12	19961220	03:53:02	−5.18	35.96	4.6	Harvard	229	57	−010	2	92	SS
13	20030614	03:10:02	−5.71	35.97	4.6	Harvard	340	26	−112	180	90	NF

(Mb): magnitude, (Strike, Dip, Slip): parameters of one of the focal plane, the second one being orthogonal, (SH_{max}, Sh_{min}): respectively, maximum and minimum horizontal principal stress directions, (Reg): stress regime according to the World Stress Map. The SH_{max}, Sh_{min} and Regime (Reg) are obtained according to the World Stress Map standard. Kebede: Kebede and Kulhanek (1991); Harvard: Harvard Centröid Moment Tensor catalogue (CMT); Brazier: Brazier et al. (2005).
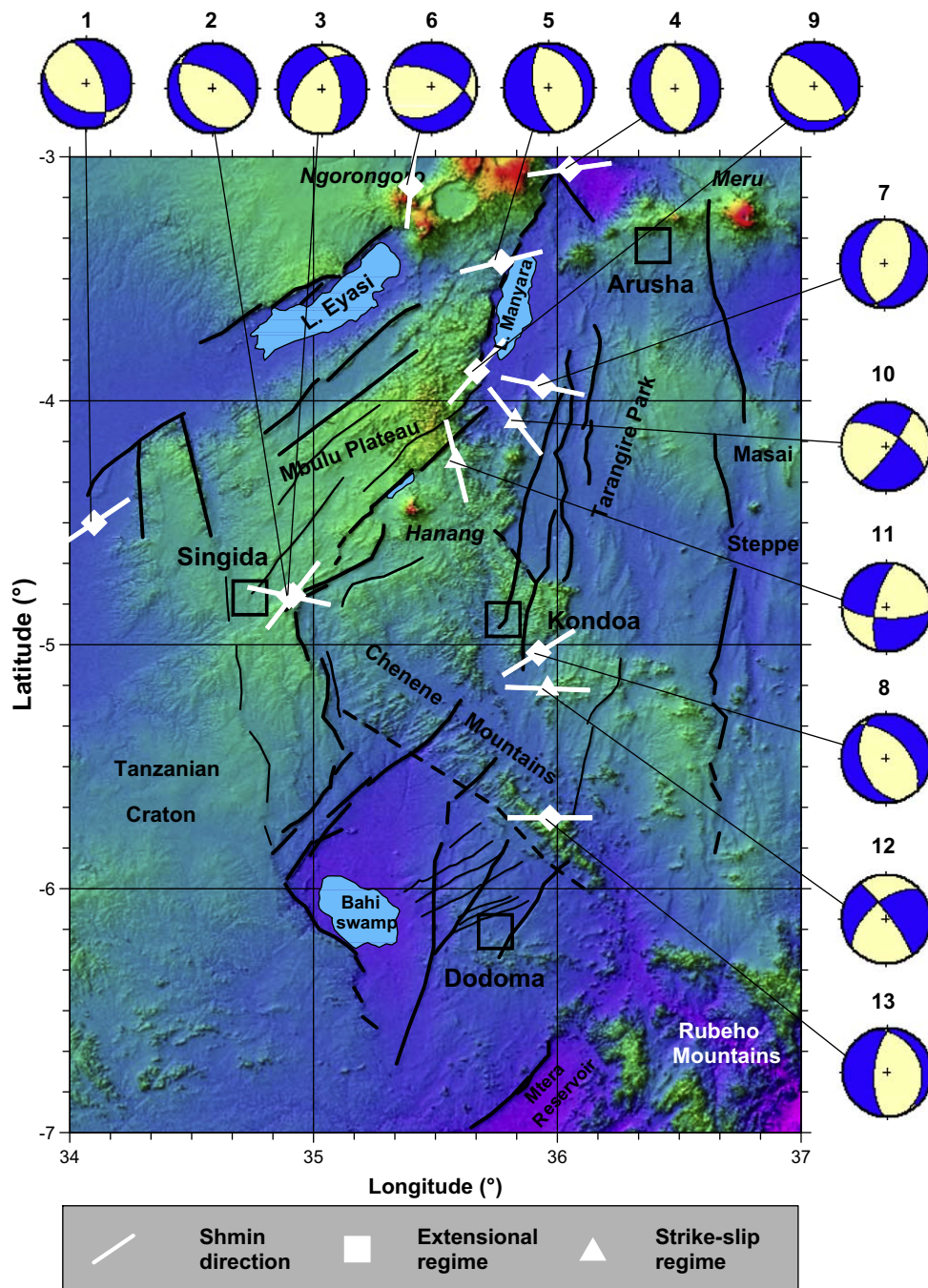
Fig. 6. Earthquake focal mechanisms map of the Manyara–Dodoma Rift segment in Central Tanzania shown on the SRTM topography as in Fig. 2. Data are from Table 2a. The horizontal principal extension direction and the stress regimes are shown according to the principle of the World Stress Map (Sperner et al., 2003). The dominant regime is normal faulting under E–W extension, but strike-slip faulting also exists.

Table 2b
Parameters of the present-day stress tensor inverted from the focal mechanism data of Table 2a

n	nt	σ_1	σ_2	σ_3	R	SD	F5	Q.R.	R'	Reg	SH_{max}	Sh_{min}
10	13	83/248	02/352	06/083	0.50	7.15	7.89	C	0.50	NF	172	82

(n): number of data used in the inversion, (nt): total number of data in the database, (σ_1, σ_2, σ_3): orientation of the three principal stress axes in *plunge/azimuth* format, (R): stress ratio, (SD): average slip deviation in degrees, (F5): misfit function, (QR): quality rank, (R'): stress regime index, (Reg): stress regime according to the World Stress Map, (SH_{max}, Sh_{min}): respectively, maximum and minimum horizontal principal stress directions.

inversion (15 data is the minimum data needed for a B quality).

In spite of the rather medium quality rank of the tensor, the stress axes appear to be stable (see [1] for the explanation of this concept). This is seen on the stability diagrams for the rotation of the tensor successively around the three principal stress axes ($-10.8/+11.7°$ rotation around σ_1, $-9.9/+9.9°$ rotation around σ_2 and $-18/+13.5°$ rotation around σ_3, Fig. 7c–e). Similarly, the Stress Ratio R has also a great stability, within a range of $-0.11/+0.12$ (Fig. 7f).

8. Paleostress analysis from geological fault-slip data

The stress inversion of brittle geological structures is performed on both slickenside data (i.e., fault planes with slip lines, with or without slip sense) and fracture data (i.e., shear and tension fractures) using the Win-Tensor program.

The brittle structural data sets used for paleostress analysis were collected along some of the major active faults surrounding the Bahi Depression: i.e., the Hombolo, Bubu and Fufu Faults (Table 3a and Fig. 8). They were measured in the footwall of the faults, in the basement rocks exposed in the fault scarps. On this basis, no relative timing control could be obtained. Only the type of fault rock might give some indications on the paleo-depth of faulting, by differentiating deep brittle (older) from shallow brittle (younger) faults. Unfortunately, no minor faults could be observed in the Quaternary sediments where a stratigraphic age control could be produced.

The reduced paleostress tensors obtained are given in Table 3b and illustrated in Fig. 8. The upper part of the Table gives the number of data used in the stress inversion (n), the total number of data measured in the outcrop (nt), the principal stress axes (σ_1, σ_2 and σ_3), the stress ratios (R) and the average slip deviation (SD). The lower part of Table 3b shows the value of the misfit function (F5), the quality rank (QR), the stress regime (Reg), the maximum horizontal principal stress direction (SH_{max}), the minimum horizontal principal stress direction (Sh_{min}) and the stress regime index (R'), in accordance with Delvaux and Sperner (2003).

---

[1] The stability for the four parameters of the stress tensor is estimated in the following way; for each stress axis, the stress tensor is rotated successively by intervals of 5°: anticlockwise ($-5°$) until $-45°$ and clockwise ($+5°$) until $+45°$. At each step, the stress tensor is applied on the data selected and the value of the optimization function (F5 in this case) is calculated. A regression curve is then fitted to the data. The results are plotted graphically with the rotation angle on the horizontal axis and the value of the function on the vertical axis (Fig. 7c–e). For stability of the R value, the whole range of possible values (0–1) is checked (Fig. 7d). The total range of function variability is defined as the difference between the minimum and maximum values of the function F5 in the stability plots, expressed in percent of the total range of function values (from 0 to the maximum). The rotation stability corresponds to the amount of rotation needed to be performed in both clockwise and anticlockwise senses along the regression curve in order that the function F5 reaches a value which is 5% higher than its minimum value. When computed this way, the clockwise and anticlockwise values for the axes stability are not necessarily identical. The same principle has been adapted for the stability of the stress ratio R.

8.1. Hombolo fault

Near the Hombolo dam, along the overflow channel, well-exposed basement rocks display different types of ductile and brittle structures. The deformation phase responsible for the formation of the ductile fabric in the biotite-rich granitic rocks is considered to be the oldest phase in the area. It is most likely Precambrian in age and attributed to a high-pressure/temperature (ductile) environment, whereas the faults and fractures formed in lower grade attributed to less confined (brittle) environments.

In a first outcrop (Fig. 8a), two types of brittle structures are observed: (1) low-angle compressional faulting, associated with Riedel shears and lunate fractures, (2) high-angle extensional faulting, associated with Fe-oxide coatings and dipping about 75°NW with a general strike around N20°E. Both types could not easily be separated in the field solely based on the presence, degree and type of mineralization. A reduced stress tensor modeled for the fault-slip data of these first two types of brittle data together gives a compressional strike-slip stress tensor with a N127°E horizontal principal compression (SH_{max}) and a R' value of 1.95 (transition between strike-slip and compressional regimes) (Table 3b).

At a different outcrop along the Hombolo dam overflow channel, where the superficial layers have been removed, some rocks appear with calcrete cement filling high-angle fractures (Fig. 8b). These are interpreted as fractures that formed close to the subsurface with alternating periods of flooding and drying, in a geographically low-relief environment. They are affecting the Plio-Quaternary sediments forming the floor of the Bahi Depression. They appear in two different families with a conjugated relationship. Slip lines could hardly be observed, but, using the law of conjugated fractures, the slip direction and sense can be reconstructed. When measuring the orientation of the two conjugated planes, special attention was paid to the proper selection of pairs of conjugated planes. Only intersecting fractures with a dihedral angle close to 60° were considered to be associated in pairs of conjugated planes. The corresponding stress inversion gives a C-quality stress tensor with an E–W sub-horizontal extension ($Sh_{min} = N104°E$). The relatively low C quality is imposed by the type of data used (mainly conjugated shear fractures), which is here the limiting factor for the quality of the tensor (Table 3b).

From the structural analysis and paleostress reconstruction, it can be concluded that the Hombolo Fault recorded at least two brittle tectonic events: an earlier (deeper) compressional event and a later (superficial) extensional event.

8.2. Bubu fault

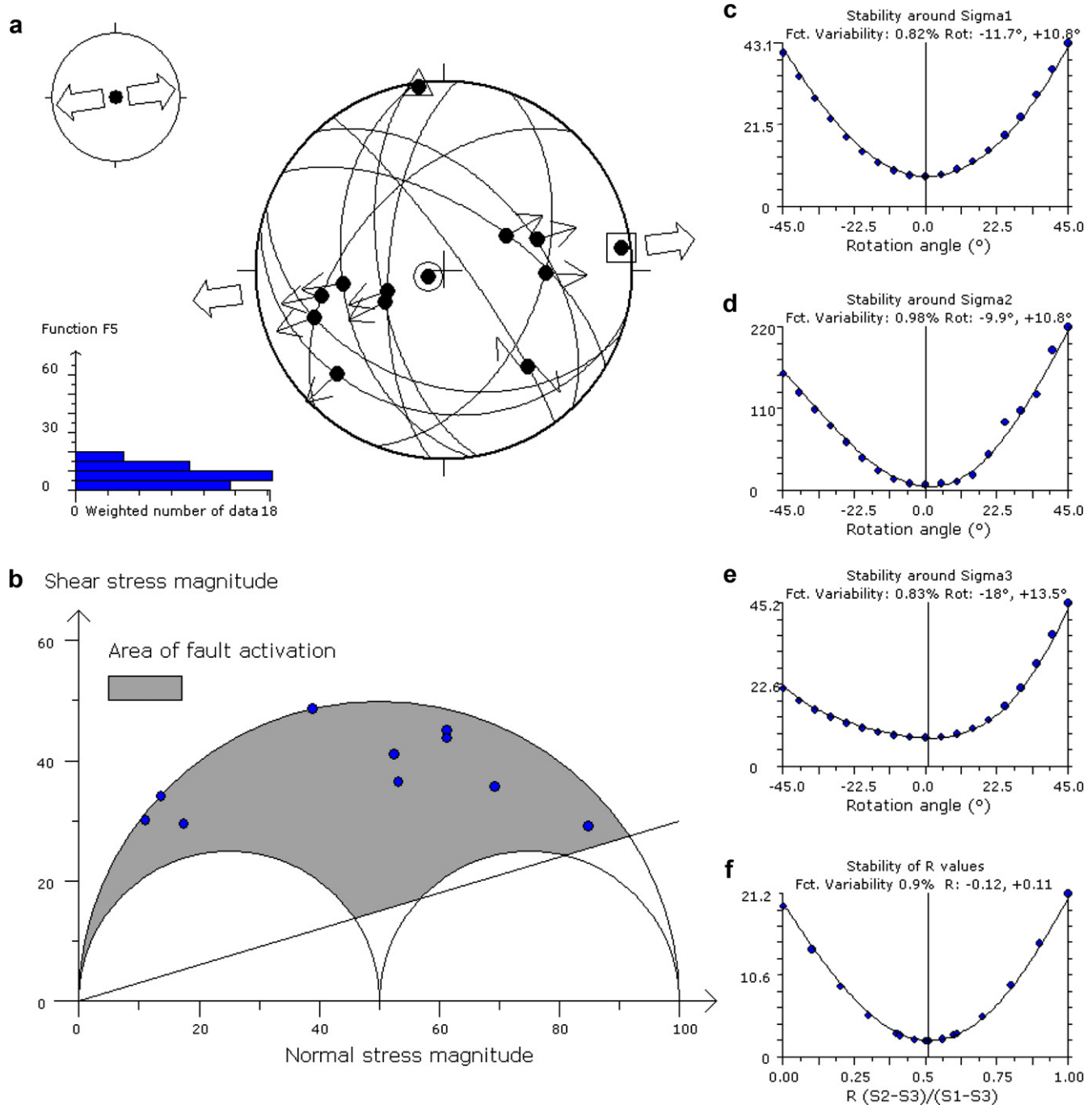Like in the Hombolo area, low-angle and high-angle faults were documented along the Makutupora segment

Fig. 7. Stress inversion of the focal mechanisms data from Table 2a. Results are given in Table 2b. (a) Lower-hemisphere Schmidt stereoplot of the selected focal planes and associated slip lines after the inversion-separation procedure. The histogram represents the distribution of the misfit function F5, weighted arithmetically according to the magnitudes. Stress symbols described in the legend of Fig. 8. (b) Mohr diagram for the stress solution. The area of possible fault activation is constrained by the three circles and the line of initial friction corresponding to an angle of 16.7°. (c–e): Stability diagrams, respectively, for σ_1, σ_2 and σ_3 axes after the inversion (explanation in text). (f): Stability diagram for the stress ratio R.

of the Bubu Fault (Fig. 8c). Stress inversion reveals a compressional regime with a marked strike-slip component ($R' = 2.11$), an E–W horizontal compression ($SH_{max} = $ N096°E) and an average medium C quality (Table 3b). The fault planes that correspond to this regime are covered by epidote, chlorite and Fe-oxides. No recent related tectonic activity was documented at this site.

Further northeast along the Bubu Fault, at the Gonga hot spring field area, the Bubu River exposes fractured granite outcrops along its banks. Most fractures are high-angle features and display no visible slip lines. Only a few fault planes with slip lines are seen to reactivate some of the sub-vertical fractures or were neoformed. The sub-vertical fractures (55 in total) were grouped into a first subset,

Table 3a
Location and description of the sites for fault kinematic and paleostress analysis

Site ID	Latitude	Longitude	UTM_X	UTM_Y	Location	Age relations	Fault type
DD824	−5.9467	35.9711	828,936	9,341,981	Hombolo (Dam)	Old event, chlorite–epidote on planes	Low angle + Riedel shears
						Related to Late Cz normal faulting	Conjugated fractures
DD830	−5.3082	35.5514	782,793	9,412,743	Bubu (Makutupora segment)	Old event, chlorite–epidote on planes	Shear fractures + faults
DD833	−5.4092	35.4647	773,243	9,401,619	Bubu (Gonga segment)	Major (older) jointing	Fractures
						Minor (younger) slip reactivations	Slickensided faults
DD864a	−6.6810	35.9590	827,190	9,260,599	Fufu fault, (main segment)	Old fractures	Shear fractures only
						Related to Late Cz normal faulting	Shear fractures + faults
DD864b	−6.6440	35.9610	827,436	9,264,693	Fufu fault (northern segment)	Related to Late Cz normal faulting	Recent faults + fractures

Coordinates in WGS84, UTM zone 36.

and considered as shear fractures (Fig. 8d). They were inverted in order to minimize the normal stress and maximize the shear stress on them. As the stress ratio cannot be constrained by fractures alone, it was fixed to 0.5 prior to the inversion. A strike-slip tensor was obtained with a NW–SE horizontal compression (SH_{max} = N142°E) and a NE-SW horizontal extension (Sh_{min} = N052°E). The tensor is stable around its vertical axis (σ_2), which means that the SH_{max} and Sh_{min} directions are well constrained, but it is less stable around the σ_3 axis. As this tensor is based solely on the inversion of shear joints, the overall rank is limited to a D quality (Table 3b).

The second subset, which contains the few fault planes with slip lines (Fig. 8e), is characterized by an E–W compression, also in a strike-slip regime with relatively oblique σ_1 and σ_2 axes (R' = 1.26, SH_{max} = N088°E, Table 3b). The tensor has a D quality due to the small number of data available (10) and data used (8). It likely represents a minor and later tectonic event relative to the generation of the sub-vertical joints.

While we attribute both paleostress tensors to pre-rift tectonic regimes, we conclude that the strike-slip regime with NW–SE horizontal principal compressional is older than the paleostress regime with E–W principal compressions.

8.3. Fufu fault

Along the main NE-trending segment of the Fufu Fault (Fufu Main), the total measured data set contains 103 fault and fracture data. According to their orientations, characteristics and interactive separation during processing, the data were separated into two subsets: i.e., one subset containing 56 sub-vertical and apparently conjugated fractures without observed slip lines (Fig. 8f) and another subset with 34 faults and fractures of a wider variety of orientations (Fig. 8g). Paleostress inversion of the first set was performed in a similar way as for the older subset of the Bubu–Gonga site, by considering the fractures as shear joints and fixing the R value to 0.5 before the inversion. Again, a strike-slip stress tensor with E–W horizontal compression (SH_{max} = N079°E) and a D quality (limited by the data type) is obtained (Fig. 8f, Table 3b).

The second set along the same segment of the Fufu Fault gives a well-constrained normal faulting regime with a N040°E horizontal extension (Sh_{min}). The quality is limited to D as the proportion of the data used (n = 34) is relatively small compared to the total fault population (nt = 103) (Fig. 8g, Table 3b).

At the northern end of the Fufu Fault (Fufu North), where it trends nearly N–S, a normal faulting regime was again found on a set of normal to oblique faults of various orientations (Fig. 8h, Table 3b). Its low R value (0.13), implies that the position of the sub-vertical σ_1-axis is well constrained, but that both the horizontal stress axes ($\sigma2$ and $\sigma3$) are not well constrained. Nevertheless, an ENE–WSW direction of horizontal extension (Sh_{min} = N067°E) is well established. The quality of this last tensor is estimated at a C rank, owing to the number of data used (n = 17), their high proportion relative to the measured data (17/19), the good spatial distribution of the fault planes and slip lines, and the low average slip deviation (SD = 3.4). Only the data type which is a combination of faults and fractures prevents it from being ranked as a B quality. These brittle structures are often associated with traces of kaolinization, but they consist to a large extent of non-mineralized joints and barren fracture planes.

9. Discussion

Investigation of the southward prolongation of the Eastern Branch of the EARS south of Lake Manyara shows that the current rift-related tectonic activity continues to the region of Dodoma. Until recently, the Eastern Branch, which is well expressed in Kenya and described there as the "Gregory Rift", is often considered to split in the North Tanzanian Divergence into three segments: the SW-trending Eyasi graben, the S-trending Natron basin and the SE-trending Pangani Rift. South of the Eyasi and Manyara grabens, the morphostructural expression of rifting becomes more discrete. The main structures are apparent on the 1:125,000 geological maps. The compilation of James (1967a) showed the Gregory rift to continue southwards to at least the Bahi Depression in the Dodoma area.

Using modern digital relief, seismological and geological data, coupled with the pre-existing knowledge, we confirm and illustrate that rift faulting and deformation extends southwards down to the region of Dodoma. In addition, we highlight the recent and present-day tectonic activity of that area and show that this current tectonic

a: Hombolo Dam (old)

b: Hombolo Dam (recent)

c: Bubu - Makutupora

d: Bubu – Gonga (Old)

e: Bubu – Gonga (Younger)

f: Fufu Main (Old)

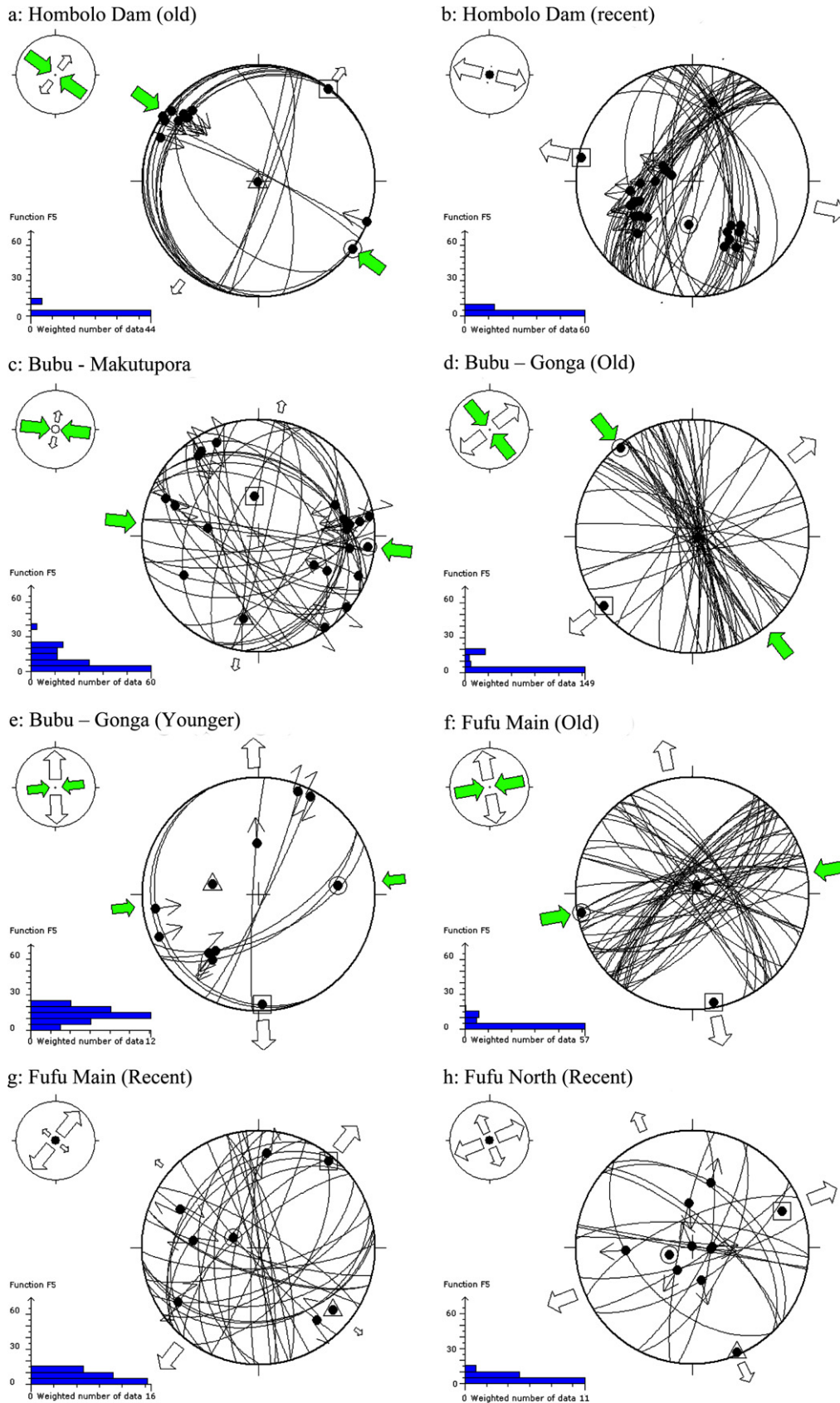g: Fufu Main (Recent)

h: Fufu North (Recent)

Fig. 8. Paleostress inversion of geological fault-slip data from the sites of Table 3a. Results are given in Table 3b. For each tensor, the results are displayed as in Fig. 7a. Stress symbols show the horizontal stress axes (SH_{max} and Sh_{min}), in function of the stress ratio R. Their length and colour symbolize the horizontal deviatoric stress magnitude, relative to the isotropic stress (σi). White outward arrows: extensional deviatoric stress ($<\sigma_i$). Black inwards arrows: compressional deviatoric stress ($>\sigma_i$). The vertical stress (σ_v) is symbolized by a solid circle for extensional regimes ($\sigma_1 = \sigma_v$), a dot for strike-slip regimes ($\sigma_2 = \sigma_v$) or an open circle for compressional regimes ($\sigma_3 = \sigma_v$).

Table 3b
Parameters of the paleostress stress tensors inverted from fault-slip data on the sites located on Table 3a

Site name	Stage	n	nt	σ_1	σ_2	σ_3	R	SD	F5
Hombolo	Old	18	80	00/126	89/216	01/037	0.05	4.3	3.65
Hombolo	Recent	52	80	59/185	30/014	03/282	0.49	6.6	3.26
Bubu–Makutopora	Old	37	43	06/096	28/190	62/354	0.11	7.8	8.79
Bubu–Gonga	Old	48	55	03/321	86/098	04/232	Fixed to 0.5	3.62	
Bubu–Gonga	Younger	8	10	32/084	57/282	06/178	0.74	4.4	12.87
Fufu (Main)	Old	56	103	04/260	84/030	05/169	Fixed to 0.5	3.37	
Fufu (Main)	Recent	34	103	71/291	18/130	05/039	0.35	1.2	3.29
Fufu (North)	Recent	17	19	73/251	02/157	18/068	0.16	3.4	4.76

Site name	Stage	QR	Reg	SH_{max}	Sh_{min}	R'	Limiting factor
Hombolo	Old	D	TS	127	037	1.95	Slip lines dispersion
Hombolo	Recent	C	NF	014	104	0.49	Data type
Bubu–Makutopora	Old	C	TF	096	006	2.11	Slip deviation
Bubu–Gonga	Old	D	SS	142	052	1.50	Data type
Bubu–Gonga	Younger	D	SS	088	178	1.26	Number of data
Fufu (Main)	Old	D	SS	079	169	1.50	Data type
Fufu (Main)	Recent	D	NF	130	040	0.35	Ratio of used data
Fufu (North)	Recent	C	NF	157	067	0.16	Data type

Description of the parameters as in Table 2b. Upper part; (n): number of data used in the stress inversion, (nt): total number of data measured in the outcrop, (σ_1, σ_2, σ_3): orientation of the principal stress axes in *plunge/azimuth* format, (R): stress ratios, (SD): average slip deviation, (F5): misfit function. Lower part; (QR): quality rank, (Reg) stress regime according to the World Stress Map, (SH_{max}, Sh_{min}): respectively, maximum and minimum horizontal principal stress directions, (R'): stress regime index, (limiting factor): the factor that is limiting the quality of the result. These parameters are described in more details in Delvaux and Sperner (2003).

deformation forms a broad zone of crustal deformation extending north-south from lakes Eyasi and Manyara to the Mtera dam reservoir, between the Tanzanian Craton on the west and the Masai Steppe on the east (Fig. 2). This zone is hereby called "Manyara–Dodoma Rift segment" and runs across Central Tanzania, along the eastern margin of the Tanzanian Craton, at its contact with the Mozambique Belt.

9.1. The Manyara–Dodoma Rift segment in Central Tanzania

Located between the North Tanzanian Divergence and the Kilombero Rift valley that has attracted attention recently (Ebinger et al., 1997; Foster et al., 1997; Tesha et al., 1997; Ring et al., 2005 for the North Tanzanian Divergence; Le Gall et al., 2004 for the Kilombero Rift valley), the Manyara–Dodoma Rift segment in Central Tanzania remained somehow neglected. Similarly, in the kinematic models and synthetic maps of the EARS (Tiercelin et al., 1988; Morley, 1999a; Chorowicz, 2005 and many others), the role of the Manyara–Dodoma segment within the dynamics of the EARS is sometimes under represented. This is probably due to the fact that these syntheses were based on the interpretation of large-scale remote-sensing images and the ETOPO30 digital database that did not show clearly the features associated with this segment. However, the existence of tectonic dislocations, thermal springs and earthquake activities were noticed by geologists that mapped the area in the years 1950–1960, and are well documented in the subsequently published geological maps. The Manyara–Dodoma Rift segment is shown

to be macro-seismically active on the maps compiled by Fairhead and Girdler (1972) and Morley (1999b), but its high level of microseismicity was only revealed by the establishment of local and temporary dense seismic network (Nyblade et al., 1996).

The present work details the structural expression of rifting south of the North Tanzanian Divergence. It shows in addition that this Manyara–Dodoma segment is particularly active as regards the presence of seismicity, fresh morphotectonic scarps displacing the Plio-Quaternary cover, warm thermal springs and open surface fractures.

In terms of rift architecture, it is difficult to consider the Eyasi and Manyara basins as two separated segments of the North Tanzanian Divergence. Instead, they both participate to the marked broadening of the territory affected by rift tectonics south of Lake Natron.

The evolution of the Dodoma–Manyara Rift segment can also be explained in terms of the two-phase rifting model formulated by Dawson (1992). The geological archives preserved as rift-related sediments, volcanics and tectonic structures all show that the rifting process was discontinuous and changed with time. The first phase of rifting, which is the longest in time and the best expressed morphologically, did not substantially affect the portion of the rift located south of the North Tanzanian Divergence (south of 4°S). The second stage, which has been proposed by Fairhead et al. (1972) and MacIntyre et al. (1974) to have started 1.2–1.3 Ma ago and is still ongoing, has extended the pre-existing fault network by a large number of new discrete faults, which have until now vertical offsets that do not exceed 200–300 m (Macheyeki et al., in press). This stage is also associated with

explosive nephelinitic volcanism in the north (e.g. the Hanang volcano), helium-bearing moderately warm thermal springs, and rather intense seismic activity of weak to moderate magnitude.

9.2. Present-day stress field and fault kinematics

The stress inversion of the available earthquake focal mechanism data shows that the present-day stress field is characterized by a pure normal faulting regime ($R' = 0.50$) and a horizontal direction of extension (Sh_{min}) at N082°E, close to E–W. This represents the average stress direction for the Manyara–Dodoma Rift segment as the available data allow calculating it. Most of the focal mechanisms included in the inversion are classified according to the Word Stress Map standard as normal faulting (NF) regime, but one of them is of strike-slip (SS) regime. Two other strike-slip mechanisms have been excluded from the database during the interactive inversion-selection procedure. Faults that are activated under a purely extensional stress regime, do not always have pure dip-slip movements. They may have a strike-slip component that can be significant depending on their orientation with respect to the three principal axes of the stress ellipsoid. In certain conditions, even sub-horizontal movements can be generated on suitably oriented sub-vertical faults. Considering the reactivation of existing planes of weakness, Bott (1959) showed that the induced slip on a fault under a particular stress field depends on the orientation of this fault plane and on the four parameters of the reduced stress tensor. As recalled above, this is the basic principle of the tectonic stress reconstruction from a data set of known fault plane and slip directions. Using the same principle, it is also possible to apply a known reduced stress tensor to a set of weak planes, and model the theoretical slip on them. In the present case, the known stress tensor would be the one inverted from the focal mechanisms that represents the modern stress field of the Manyara–Dodoma Rift segment. The planes of weakness are selected in order to represent the most frequently observed active structural trends, to which a dip-angle of 60° is imposed (reflecting the dominant normal faulting mechanism of the region). As a result (Fig. 9a, Table 4), all the computed slip directions show a dominant normal dip-slip component of movement, but a strike-slip component is also present, the importance of which depends on the orientation of the given faults with respect to the horizontal direction of principal extension (Sh_{min}). If the dip angles of some faults, which are highly oblique to Sh_{min} (e.g. Bahi Fault and northern part of Bubu Fault in the Bahi Depression, ...), are set at angles higher than 60°, the resulting slip on them would tend to be even more strike-slip. In the shear stress τ versus normal stress σ_n Mohr diagram (Fig. 9b), all data plot above the line of initial friction corresponding to the initial friction angle of 16.7° (Byerlee, 1978) and are thus likely to be reactivated.

9.3. Slip-tendency analysis

The potential activity of these faults can be further estimated using the principle of slip-tendency analysis which permits to rapidly assess the stress state on a fault (Morris et al., 1996). The likelihood that slip will occur on a given surface under a given stress field depends on its frictional characteristics and the ratio of shear to normal stress acting on this surface. Slip will occur if the resolved shear stress exceeds the frictional resistance to sliding, which is proportional to the normal stress acting across that surface. In other words, slip will be favored on those faults that have an orientation resulting in the highest shear stress τ and the lowest normal stress σ_n on the fault plane. The magnitude of these resolved stresses depends solely on the stress field and the orientation of the faulted surface. In Table 4, the relative magnitudes of the normal stress (σ_n) and shear stress (τ), the friction angle $\Omega = \arctan \tau/\sigma_n$ and the slip tendency $T_s = \tau/\sigma_n$ are given for each fault under the modeled stress tenors. The relative magnitudes are computed for given arbitrary magnitudes of $\sigma_1 = 100$ and $\sigma_3 = 0$. The parameter T_s of Morris et al. (1996) is equivalent to the classical coefficient of internal friction μ. The estimated reactivation likelihood is proportional to T_s.

The slip tendency analysis considers implicitly that the slip movements occur along faults that are reactivating existing planes of weakness and, consequently, are not newly formed in a mechanically homogeneous intact medium. In the present case, the lozenge-shaped fault pattern defined by the orientation of the basement shear zones, dolerite dikes and associated fractures (NE- and NW-trends) present the lowest reactivation likelihood (e.g. the main segment of the Fufu Fault) whereas the newly formed N–S and still weakly expressed N–S faults, the highest likelihood. The main conclusions drawn from the slip-tendency analysis are:

1. the faults reactivating the NE-trend of basement dolerite dikes and associated fractures represent the lowest reactivation likelihood (Balangida South and Bubu North faults);
2. medium reactivation likelihood is obtained for the NW-trending faults, like the Bahi and Sanzawa faults, and the NNE-trending Balangida North, Saranda, Bubu South and Central faults (Fig. 10);
3. high slip tendency is given to the almost N-trending northern extremity of the Fufu Fault, and the NNW-trending Kondoa, Dodoma South, Dodoma–Kigwe and Hombolo faults. The NNW-trending Mponde Fault has the highest slip tendency of all faults analyzed as it trends almost orthogonal to the Sh_{min} direction.

Interestingly, the thermal springs are all located along faults that have a medium to high slip probability, with a high concentration in the Mponde graben (except for the Gonga springs along the Bubu Fault in the Chenene block). Although the Sanzawa Fault, separating the Chen-
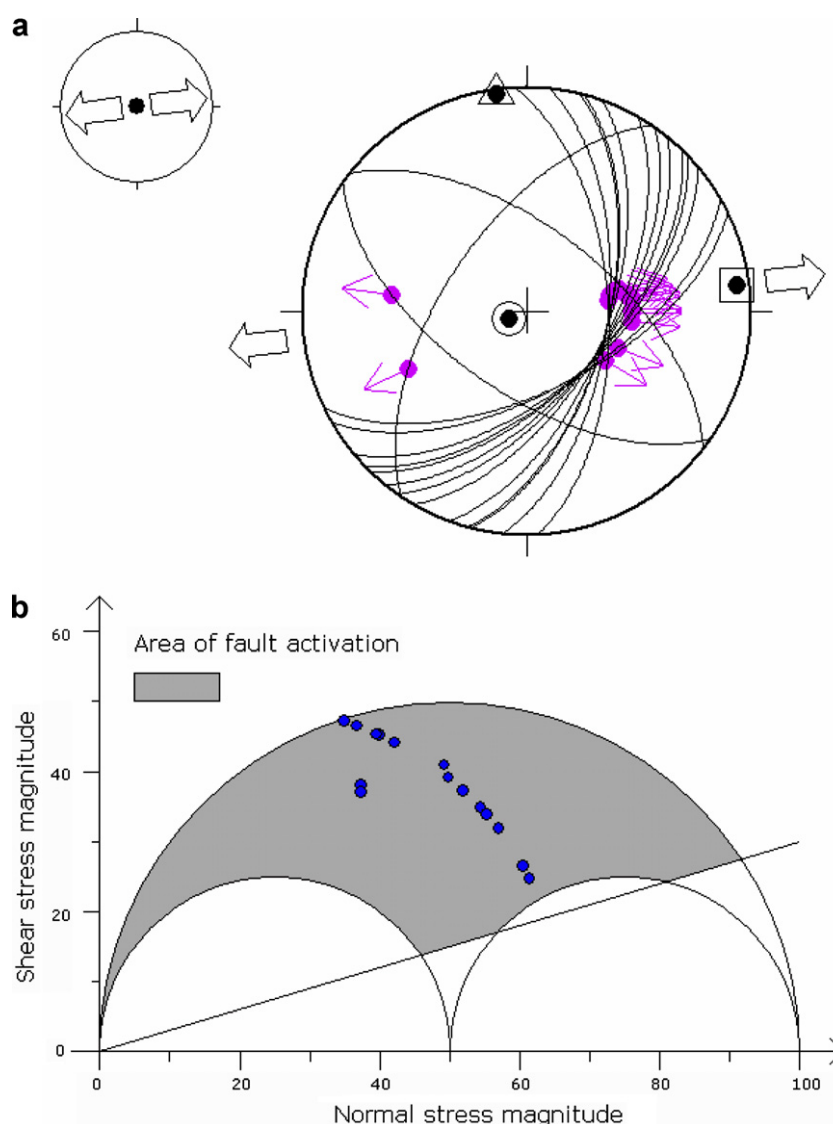
Fig. 9. Application of stress tensor to selected regional faults. Data are from Table 4. (a) Lower-hemisphere Schmidt stereoplot of the regional faults with their modeled slip. Stress symbols described in the legend of Fig. 8. (b) Corresponding Mohr diagram. All faults plot above the line of initial friction (16.7° angle), between the $\sigma_3 - \sigma_1$ circle and the $\sigma_2 - \sigma_1$ circle. The faults with the highest reactivation likelihood are closer to the external circle ($\sigma_3 - \sigma_1$) and those with the lowest reactivation likelihood are closer to the internal ($\sigma_2 - \sigma_1$) circle. On the normal stress magnitude scale, $\sigma_1 = 100$, $\sigma_3 = 0$ and $\sigma_2 = R \times 100$ where $R = \sigma_2 - \sigma_3/\sigma_1 - \sigma_3$.

ene Mountains from the Bahi Depression, has been active in the past, no clear signs of recent reactivation are seen in the field in spite of its modeled medium slip tendency.

9.4. Tectonic stress from geological data

All fault-slip data were measured in basement rocks and therefore their relative age determination is difficult. Some of the stress tensors obtained are associated with fractures and faults that appear to have the same trend as the dominant, brittle to brittle-ductile basement discontinuities. This is a common situation, when working in basement rocks affected by pre-existing tectonic deformations that were subsequently reactivated by more superficial faulting. The younger fault structures were generated when the

faulted rocks were in a more superficial position than when they were deformed in brittle to semi-brittle conditions for the first time. The brittle microstructures associated with the older (and deeper) stage of faulting are generally better expressed and much more numerous than the ones associated with active (and superficial) faulting. Therefore, when investigating the fault kinematics for paleostress reconstruction of Late Cenozoic-Quaternary deformation in basement rocks, it is not possible to ignore the older stages of faulting. It is even more important to well constrain the older deformation stages in order to isolate and separate them from the effects of the more recent deformation.

The present results show that the current extensional stress regime was preceded by a period characterized by thrusting and strike-slip, or both. Thrusting is most likely

Table 4
Resolved stress on the regional faults by the application of the present-day regional stress tensor determined from the inversion of earthquake focal mechanisms

Given fault		Computed shear stress					Slip tendency	
Name	Orientation	Shear direction	Shear sense	N_{mag}	T_{mag}	FA	T_s	Likelihood
Balangida South	60/154	56/122	NS	60.1	25.6	23.1	0.43	Low
Bubu North	60/150	54/112	NS	59	27.6	25.1	0.47	Low
Balangida North	60/144	51/096	NS	55.3	33	30.8	0.6	Medium
Bubu Centre	60/136	51/091	NS	53.5	35.1	33.3	0.66	Medium
Fufu Main	60/134	51/089	NS	52.5	36.1	34.5	0.69	Medium
Saranda	60/129	51/085	NS	50.1	38.4	37.5	0.77	Medium
Bahi	60/038	51/083	ND	51.8	40.2	37.8	0.78	Medium
Bubu South	60/125	52/082	NS	48.1	40.1	39.8	0.83	Medium
Dodoma North	60/120	53/080	NS	45.6	41.9	42.6	0.92	Medium
Sanzawa	60/215	39/277	ND	38.6	35.9	43	0.93	Medium
Dodoma South	60/110	55/077	NS	40.9	44.7	47.5	1.09	High
Hombolo	60/304	41/244	NS	34.9	38.8	48	1.11	High
Fufu North	60/105	57/077	NS	39	45.7	49.5	1.17	High
Kondoa	60/104	57/077	NS	38.7	45.8	49.9	1.18	Highest
Dodoma–Kigwe	60/096	59/079	NS	36.4	46.9	52.2	1.29	Highest
Mponde	60/087	60/083	NS	35.2	47.6	53.5	1.35	Highest

Parameters of the regional stress tensor are from Table 2b. The orientations of the fault planes are in *dip/dip direction* format, and those of the shear direction in *plunge/azimuth* format. Shear sense: NS – normal with a sinistral component, ND – normal with a dextral component. (N_{mag} and T_{mag}): normal and shear stress magnitudes within an arbitrary scale where the magnitude of $\sigma_1 = 100$ and the magnitude of $\sigma_3 = 0$, (FA): friction angle, (T_s): slip tendency according to Morris et al. (1996). The reactivation likelihood is proportional to T_s.

the oldest tectonic regime. The strike-slip regimes described above are attributed to the Neoproterozoic (800–650 Ma) Pan-African collisional events (Mozambique Belt) that involved West and East Gondwana (e.g. Stern, 1994; Fritz et al., 2005). The Mozambique Belt is a N–S striking orogen, which thrusted against the Archaean Tanzanian Craton. Structural investigations give a clear picture of westward thrusting of the entire orogen onto the craton as a nape pile with foliation patterns showing a predominantly W–E lineation and an eastward dip direction (Fritz et al., 2005). This means that although the craton was already stable at that time (e.g., Condie, 1994), it subsequently suffered some degree of deformation.

For the recent rifting stage, although our data set is limited, we already observe a certain correlation between the youngest fault kinematics and stress tensors derived from geological observations and those derived from earthquake focal mechanism data. The convergence of the results obtained from two independent data sources, sampling very different volumes of rock and covering different periods of time is a good indication that the present-day kinematics in the Dodoma area is dominated by normal faulting under N80°E horizontal principal extension, with a strong influence of the pre-existing basement discontinuities that are reactivated obliquely to the direction of principal extension.

9.5. Rift architecture and fault kinematics

For the first stage of rifting (Late Miocene to Early Pleistocene), the state of stress is not illustrated by our data as this stage is not well expressed in the investigated region. This first stage was responsible for the formation of the Eyasi and Manyara grabens and associated fault scarp on their western side.

The second rifting stage (Mid Pleistocene – Holocene) is marked by the appearance of a new stress system, owing to further development of the rift by: (i) reactivation of the pre-existing tectonic planes of weakness of possible late Pan-African origin, and (ii) the progressive (still ongoing) development of a new fault system in a more N–S trend. This embryonic fault system develops through the appearance of new faults (near Kondoa, in the Tarangire park, and surrounding Dodoma), or by the linkage of existing rift faults (inherited from the first rift stage?) into a long chain of zig-zag faults (the Lake Manyara–Balangida–Mponde–Saranda–Bubu–Bahi fault system), mainly dipping to the East (NE, E or SE). The newly formed NNW-trending faults also tend to merge together across the Chenene blocks. The strong tectonic activity in the Chenene Mountains is likely to reflect this mechanism (e.g., the possible occurrence of recent surface dislocations observed by local farmers around Chenene village).

The current rifting process is causing a structural reorganization of the rift architecture by the progressive alignment of the pre-existing faults towards parallelism with the N–S rift axis (e.g. as discussed in McClay and White, 1995).

In terms of rift architecture, Le Gall et al. (2004) suggest that the link between the Eastern Branch of the EARS in North Tanzania and the Mikumi–Kilombero reactivated Karoo Rift is expressed by the SW-trending basement high formed by the Chenene Mountains (so-called Maminzi–Tagalala fault zone), running between the Balangida fault in the North and trough the Rubeho Mountains and join-
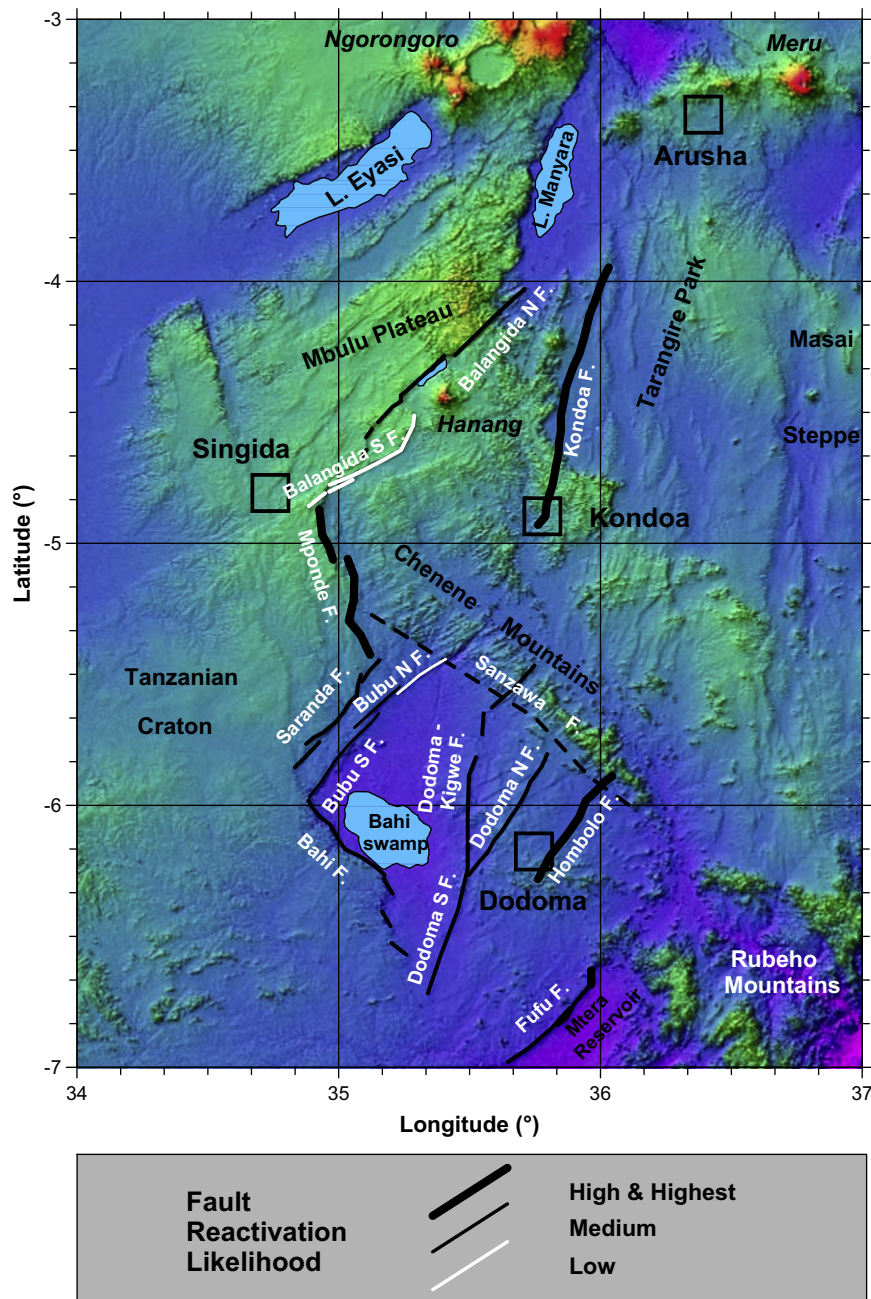
Fig. 10. Reactivation likelihood of selected regional faults as a result of the slip tendency analysis, displayed on the SRTM topography as in Fig. 2. Only faults considered in this analysis are displayed.

ing the Mikumi depression in the South (Figs. 1, 2). This might be true for the first rift stage, but our data suggest that it is no more the case during the second and still active rift stage. The Sanzawa scarp separating the Chenene Mountains from the Bahi Depression (Fig. 3) shows no morphological evidence for recent activation and there was even a debate about the existence of the Sanzawa Fault under the recent alluviums (Fozzard, 1961). Instead, we have shown that the Chenene Mountains are cut across at high angle to its trend by recent faults and open fractures, still weakly expressed morphologically but highlighted by elongated seismic swarms (Fig. 5).

9.6. Implications for seismic risk assessment in the Dodoma region

An important practical outcome of this work is the confirmation that the Dodoma area is not a tectonically quiet place. It is located within the still incipient, but seismically very active Manyara–Dodoma Rift segment, which forms the southward continuation of the Eastern Branch of the EARS, better expressed in northern Tanzania and in Kenya. When looking at the population density map of Tanzania (Tanzanian 2002 Population and Housing Census), it appears that generally – and in the Manyara–Dodoma

region in particular – the population is concentrated on the territories of both the Western and the Eastern Branches of the EARS surrounding the Tanzanian Craton. For different reasons, the physical environment in those regions seems more attractive, but it has obvious drawbacks in terms of risks related to natural hazards. The conjunction of a relatively high population density and increased seismic hazard makes the Manyara–Dodoma region at risk for strong earthquakes. In spite of the scientific knowledge, that this region is seismically active, the 2002 Dodoma earthquake sequence came as a surprise to the Tanzanian government and population. This region requires therefore further work to evaluate the occurrence of past strong earthquakes (paleoseismic investigations), seismic hazard assessment and site effect evaluation. It requires also the elaboration of policies for public awareness rising and of seismic risk mitigation.

10. Conclusion

The Eastern Branch of the East African Rift System continues southwards after the North Tanzanian Divergence in a broad N–S trending and active deformation zone. This zone, which includes both the Eyasi and Manyara grabens, forms the so-called "Manyara–Dodoma" rift segment. In a two-stage rifting model, most part of these rift structures represent the southward expansion of the Eastern Branch during the second rift stage, which is thought to have started in the Middle Pleistocene (at about 1.3–1.2 Ma ago).

Reconstruction of tectonic stress from geological fault and fracture data gives mainly stress tensors that are likely related to the late tectonic stages of the Pan-African Mozambique orogeny. The present-day stress field determined from earthquake focal mechanisms is of typical normal faulting regime, with a nearly E–W direction of horizontal extension. Slip-tendency analysis shows that the newly developing N–S to NNE-trending faults have the highest slip tendency. The current rifting stage is responsible for the structural reorganization of the rift architecture by progressive alignment of the pre-existing faults towards parallelism with the N–S rift axis and linking the once isolated rift faults into long chains of zig-zag faults. Those are marked by the distribution of earthquakes swarms, hot springs, fresh morphotectonic scarps and open fractures.

The ongoing tectonic process in the Manyara–Dodoma Rift segment makes this region at risk for moderate to strong earthquakes. This requires policies to be developed for the mitigation of the seismic risk, particularly for the growing capital of Dodoma.

Acknowledgements

References

Angelier, J., 1989. From orientation to magnitudes in paleostress determinations using fault slip data. Journal of Structural Geology 11, 37–50.

Angelier, J., 1994. Fault slip analysis and paleostress reconstruction. In: Hancock, P.L. (Ed.), Continental Deformation. Pergamon, Oxford, pp. 01–120.

Atmaoui, N., Hollnack, D., 2003. Neotectonics and extension direction in the Southern Kenya Rift, Lake Magadi area. Tectonophysics 364, 71–83.

Arad, A., Morton, W.H., 1969. Mineral springs and saline lakes of the Western Rift Valley, Uganda. Geochemica et Cosmochimica Acta 33, 1169–1181.

Barth, H., 1996. Gold in the Dodoman Basement of Tanzania, Hanover, 53p.

Bell, K., Dodson, H.S., 1981. The geochronology of the Tanzania shield. Journal of Geology 89 (1), 109–128 (Chicago).

Bosworth, W., Strecker, M.R., Blisniuk, P.M., 1992. Integration of East African paleostress and present-day stress data: implications for continental stress field dynamics. Journal of Geophysical Research 97 (B8), 11851–11865.

Bott, M.H.P., 1959. The mechanisms of oblique slip faulting. Geological Magazine 96, 109–117.

Brazier, R.A., Nyblade, A.A., Florentin, J., 2005. Focal mechanisms and stress regime in NE and SW Tanzania, East Africa. Geophysical Research Letters 32/14 (1–4).

Brown, C., Girdler, R.W., 1980. Interpretation of African Gravity and its implication for the breakup of the continents. Journal of Geophysical Research 85 (Ba), 6443–6455.

Byerlee, J.D., 1978. Friction of rocks. Pure and Applied Geophysics 116, 615–626.

Calais, E., Ebinger, C., Hartnady, C., Nocquet, J.M., 2006. Kinematics of the East African Rift from GPS and earthquake vector data. In: Yirgu, G., Ebinger, C.J., Maguire, P.K.H. (Eds.), The Afar Volcanic Province Within the East African Rift System, vol. 253. Geological Society of London, Special Publication, pp. 9–22.

Chorowicz, J., 2005. The East African rift system. Journal of African Earth Sciences 43, 379–410.

Condie, K.C., 1994. Archean Crustal Evolution. Elsevier Science, New York.

Dawson, J.B., 1992. Neogene tectonics and volcanicity in the North Tanzania sector of the Gregory Rift Valley: contrasts with the Kenya sector. Tectonophysics 204, 81–92.

Deino, A., Tauxe, L., Monaghan, M., Drake, R., 1990. ^{40}Ar/^{39}AR calibration of the litho- and palaeomagnetic stratigraphies of the Ngorora Fm., Kenya. Journal of Geology 98, 567–587.

Delvaux, D., 1991. The Karoo to Recent rifting in the western branch of the East-African Rift System: a bibliographical synthesis. Mus. Roy. Afr. Centr., Tervuren (Belgique), Dép. Géol. Min., Rap. Ann. 1989–1990, pp. 63–83.

Delvaux, D., Hanon M., 1993. Neotectonics of the Mbeya area, SW Tanzania. Mus. Roy. Afr. Centr., Tervuren (Belgique), Dép. Géol. Min., Rap. Ann. 1991–1992, pp. 87–97.

Delvaux, D., Levi, K., Kajara, R., Sarota, J., 1992. Cenozoic paleostress and kinematic evolution of the Rukwa–North Malawi rift valley (East African rift system). Bulletin du Centre de Recherches elf Exploration Production elf Aquitaine (16/2), 383–406.

Delvaux, D., Moeys, R., Stapel, G., Petit, C., Levi, K., Miroshnichenko, A., Ruzhich, V., Sankov, V., 1997. Paleostress reconstructions and geodynamics of the Baikal region, Central Asia. Part II: Cenozoic rifting. In: Structural Controls on Sedimentary Basin Formation. Cloetingh, S., Fernandez, M., Munoz, J.A., Sassi, W., Horvath, F. Tectonophysics 282, 1–38.

Delvaux, D., Sperner, B., 2003. Stress tensor inversion from fault kinematic indicators and focal mechanism data: the TENSOR program. In: Nieuwland, D. (Ed.), New Insights into Structural Interpretation and Modelling, vol. 212. Geological Society of London, Special Publication, pp. 75–100.

Dunne, W.M., Hancock, P.L., 1994. Paleostress analysis of small-scale brittle structures. In: Hancock, P.L. (Ed.), Continental Deformation. Pergamon, Oxford, pp. 01–120.

Ebinger, C.J., 1989. Tectonic development of the western branch of the East African rift system. Bulletin of the Geological Society of America 101, 885–903.

Ebinger, C.J., Deino, A.L., Drake, R.E., Thesa, A.L., 1989. Chronology of vulcanism and rift basin propagation: Rungwe volcanic provinces, East Africa. Journal of Geophysical Research 94, 15.783–15.803.

Ebinger, C., Poudjom Djomani, Y., Mbede, E., Foster, A., Dawson, J.B., 1997. Rifting Archaean lithosphere: the Eyasi–Manyara–Natron rifts, East Africa. Journal of the Geological Society of London 154, 947–960.

Fairhead, J.D., Girdler, R.W., 1972. The seismicity of the East-African rift system. Tectonophysics 41, T19–T26.

Fairhead, J.D., Mitchell, J.G., Williams, L.A.J., 1972. New K/Ar determinations on Rift volcanics of South Kenya and their bearing on the age of Rift faulting. Nature 238, 66–69.

Fairhead, J.D., Stuart, G.W., 1982. The seismicity of the East-African rift system and comparison with other continental rifts. In: Palmason, G. (Ed.), Continental and Oceanic Rifts. Geodynamic Series 8, 41–61.

Fawley, A.P., 1956. Diamond drilling in the Bahi Swamp. Records of the Geological Survey of Tanganyika 6, 47–51.

Fernandez-Alonso, M., Delvaux, D., Klerkx, J., Theunissen, K., 2001. Structural link between Tanganyika- and Rukwa-rift basins at Karema-Nkamba (Tanzania): basement structural control and recent evolution. Mus. Roy. Afr. Centr., Tervuren (Belgique), Dép. Géol. Min., Rap. Ann., 91–100.

Foster, A., Ebinger, C., Mbede, E., Rex, D., 1997. Tectonic development of the northern Tanzanian sector of the East African Rift System. Journal of the Geological Society of London 154, 689–700.

Foster, A.J., Jackson, J.A., 1998. Source parameters of large African earthquakes; implications for crustal rheology and regional kinematics. Geophysical Journal International 134, 422–448.

Fozzard, P.M.H., 1959. The Geology of the Mpondi river area: Quarter Degree Sheet 123 (41 NW.), Kwa Mtoro. Records of the Geological Survey of Tanganyika 9, 10–12.

Fozzard, P.M.H., 1961. Geological survey of Tanzania. 1:125,000 Geological map Quarter Degree Sheet 123 Kwa Mtoro. Geological Survey Division, Dodoma.

Fozzard, P.M.H., 1962. Brief explanation of the geology of QDS177 Manzoka – Geological Survey of Tanganyika, 1–7, Unpublished Report, Dodoma.

Fritz, H., Tenczer, V., Hauzenberger, C., Wallbrecher, E., Hoinkes, G., 2005. Central Tanzanian tectonic map: a step forward to decipher Proterozoic structural events in the East African Orogen. Tectonics 24, TC6013, 26p. doi:10.1029/2005TC001796.

Gabert, G., 1973. Uber Granitische Gesteine des Dodoman und Usagaran im Sudlichen Hochland von Tanzania-Geologicaljb.b. 6, 1–50, Hannover.

Gabert G., Wendt, I., 1974. Datierung von Granitischen Gesteinen im Dodoman -und Usagaran System und in Der ndembera-serie (Tanzania). Geological jaarbuch 11, 3–55, Hannover.

Harris, J.F., 1958. Geological investigations, sampling and diamond-drilling at Manyeghi Helium-bearing hot springs, Singida districs. Records of the Geological Survey of Tanganyika 8, 86–98.

Harris, J.F., 1959. Analysis of natural gases and accompanying spring waters. Records of the Geological Survey of Tanganyika 9, 94.

Hochstein, M.P., Temu, E.P., Moshy, C.M.A., 2000. Geothermal resources of Tanzania. In: Proceedings of the World Geothermal Congress, Kyushu-Tohoku, Japan, May 28–June 10, pp. 1233–1238.

Hollnack, D., Stangl, R., 1998. The seismicity related to the southern part of the Kenya rift. Journal of African Earth Sciences 26, 477–495.

Ibs-von Seht, M., Blumenstein, S., Wagner, R., Hollnack, D., Wohlenberg, J., 2001. Seismicity, seismotectonics and crustal structure of the southern Kenya Rift-new data from the Lake Magadi area. Geophysical Journal International 146, 439–453.

Iranga, M.D., 1992. Seismicity of Tanzania: distribution in time, space, magnitude, and strain release. Tectonophysics 209, 313–320.

James, J.F., 1957. Analysis of natural gases and accompanying spring waters. Records of the Geological Survey of Tanganyika 7, 104–106.

James, J.F., 1958. Analysis of natural gases and accompanying spring waters. Records of the Geological Survey of Tanganyika 8, 112–113.

James, T.C., 1967a. Thermal springs in Tanzania. Institution of Mining and Metallurgy, Transactions/Section B (Applied Earth Science) 76, B1–B18.

James, T.C., 1967b. Thermal springs in Tanzania – discussions and conclusions. Institution of Mining and Metallurgy, Transactions/Section B (Applied Earth Science) 76, B168–B174.

Kebede, F., Kulhanek, O., 1991. Recent seismicity of the East African Rift system and its implications. Physics of the Earth and Planetary Interiors 68, 259–273.

Le Gall, B., Gernigon, L., Rolet, J., Ebinger, C., Gloaguen, R., Nilsen, O., Dypvik, H., Deffontaines, B., Mruma, A., 2004. Neogene-Holocene rift propagation in central Tanzania: morphostructural and aeromagnetic evidence from the Kilombero area. Geological Society of Africa Bulletin 116 (3/4), 490–510.

Lubala, R.T., Rafoni, A., 1987. Pétrologie et signification géodynamique du volcanisme alcalin mio-pliocène de la région du lac Natron (Rift ext-africain, Tanzanie). Sciences géologiques 40 (1-2), 41–55 (Strasbourg).

Macheyeki, A.S., Delvaux, D., De Batist, M., Mruma, A., in press. Active faults and fault segmentation in the Dodoma area, Tanzania: a first assessment of the seismic hazard in the area. Journal of Tanzanian Earth Sciences.

MacIntyre, R.M., Mitchell, J.G., Dawson, J.B., 1974. Age of the fault movements in the Tanzanian sector of the East African rift system. Nature 247, 354–356.

McClay, K.R., 1987. The Mapping of Geological Structures. Open University Press & Halseted Press, Toronto, New York.

McClay, K.R., White, M.J., 1995. Analogue modelling of orthogonal and oblique rifting. Marine and Petroleum Geology 12, 137–151.

McConnell, R.B., 1972. Geological development of the rift system of eastern Africa. Bulletin of the Geological Society of America 83, 2549–2572.

Morley, C.K., 1999a. Tectonic evolution of the East African Rift System and the modifying influence of magmatism: a review. Acta Vulcanologia 11 (1), 1–19.

Morley, C.K., 1999b. Introduction to the East African rift system. In: Morley, C.K. (Ed.), Geoscience of Rift Systems – Evolution of East Africa, vol. 44. AAPG Studies in Geology, pp. 1–18.

Morris, A., Ferrill, D.A., Henderson, D.B., 1996. Slip-tendency analysis and fault reactivation. Geology 24 (3), 275–278.

Mruma, A.H., 1995. Stratigraphy and palaeodepositional environment of the Palaoproterozoic volcano-sedimentary Konse Group in Tanzania. Journal of African Earth Sciences 21 (2), 281–290.

Mugisha, F., Ebinger, C.J., Strecker, M., Pope, D., 1997. Two-stage rifting in the Kenya rift: implications for half-graben models. Tectonophysics 278, 63–81.

Nyblade, A.A., Birt, C., Langston, C.A., Owens, T.J., Last, R.J., 1996. Seismic experiment reveals rifting of craton in Tanzania. Eos Transactions AGU 77, 517–521.

Nyblade, A.A., Brazier, R.A., 2002. Precambrian lithospheric controls on the development of the East African rift system. Geology 30, 755–758.

Nyblade, A.A., Pollack, H.N., 1992. A gravity model for the lithosphere in western Kenya and northern Tanzania. Tectonophysics 212, 257–267.

Petit, J.P., 1987. Criteria for the sense of movement on fault surfaces in brittle rocks. Journal of Structural Geology 9, 597–608.

Pinna, P., Muhongo, S., Mcharo, A., Le Goff, E., Deschamps, Y., Ralay, F., Milesi, J.P., 2004. 1:2,000,000 Geology and Mineral Map of Tanzania. BRGM, Orléans, France.

Ring, U., Betzler, C., Delvaux, D., 1992. Normal vs. strike-slip faulting during rift development in East Africa: the Malawi rift. Geology 20, 1015–1018.

Ring, U., Schwartz, H.L., Bromage, T.G., Sanaane, C., 2005. Kinematic and sedimentological evolution of the Manyara Rift in northern Tanzania, East Africa. Geological Magazine 142 (4), 355–368.

Selby, J., Mudd, G.C., 1965. Geological Survey of Tanzania. 1:125,000 Geological Map Quarter Degree Sheet 104 Kondoa. Geological Survey Division, Dodoma.

Strecker, M.R., Blisniuk, P.M., Eisbacher, G.H., 1990. Rotation of extension direction in the central Kenya Rift. Geology 18, 299–302.

Shudofsky, G.N., Cloetingh, S., Stein, S., Wortel, R., 1987. Unusually deep earthquakes in East Africa: constraints on the thermo-mechanical structure of a continental rift system. Geophysical Research Letters 14, 741–744.

Sperner, B., Müller, B., Heidbach, O., Delvaux, D., Reinecker, J., Fuchs, K., 2003. Tectonic stress in the Eath's crust: advances in the World Stress Map project. In: Nieuwland, D. (Ed.), New Insights into Structural Interpretation and Modelling, vol. 212. Geological Society of London, Special Publication, pp. 101–116.

Stern, R.J., 1994. Arc assembly and continental collision in the Neoproterozoic East African Orogen: implications for consolidation of Gondwanaland. Annual Review Earth and Planetetary Sciences 22, 319–351.

Tesha, A.L., Nyblade, A.A., Keller, G.R., Doser, D.I., 1997. Rift localization in suture-thickened crust: evidence for Bouguer gravity anomalies in northeastern Tanzania, East Africa. Tectonophysics 278, 315–328.

Thomas, C.M., 1963. Geological Survey of Tanzania. 1:125,000 Geological Map Quarter Degree Sheet 84 Hanang. Geological Survey Division, Dodoma.

Tiercelin, J.-J., Chorowicz, J., Bellon, H., Richert, J.-P., Mwambene, J.T., Walgenwitz, F., 1988. East African rift system: offset, age and tectonic significance of the Tanganyika–Rukwa–Malawi intracontinental fault zone. Tectonophysics 148, 241–252.

Vogt, M., Kröner, A., Poller, U., Sommer, H., Muhongo, S., Wingate, M.T.D., 2006. Archaean and Palaeoproterozoic gneisses reworked during a Neoproterozoic (Pan-African high-grade event in the Mozambique belt of East Africa: Structural relationships and zircon ages from Kidatu area, central Tanzania. Journal of African Earth Sciences 45 (2), 139–155.

Wades, F.B., Oates, F., 1938. An explanation of degree sheet no. 52, Dodoma-Geological Survey of Tanganyika. Short paper 17, 1–60, Dar es Salaam.

Walker, B.G., 1969. Springs of deep seated origin in Tanzania. Proceedings of the XXIII International Geological Congress 19, 171–180.

Wallace, R.E., 1951. Geometry of shearing stress and relation to faulting. Journal of Structural Geology 59, 118–130.

Wendt, I., Besang, C., Kreuzer, H.,, Muller, P., 1972. Age determination of granitic intrusions and metamorphic events in the early precambrian of Tanzania. In: Proceedings of the 24th International Geological Congress, Montreal, Section 1, pp. 295–314.

Weeraratne, D.S., Forsyth, D.W., Fischer, K.M., Nyblade, A.A., 2003. Evidence for an upper mantle plume beneath the Tanzanian Craton from Rayleigh wave tomography. Journal of Geophysical Research 108 (B9), 2427. doi:10.1029/2002JB002273.

Wilkinson, P., Mitchell, J.G., Cattermole, P.J., Downie, C., 1986. Volcanic chronology of the Meru-Kilimanjaro region, Northern Tanzania. Journal of the Geological Society of London 143, 601–605.

Zoback, M.L., 1992. First- and second-order patterns of stress in the lithosphere: The World Stress Map Project. Journal of Geophysical Research 97, 11703–11728.